DEVELOPMENT OF KINETIC MODEL REDUCTION FRAMEWORK AND ITS APPLICATION IN REALISTIC FLOW SIMULATION

by

KAIYUAN HE

A Dissertation submitted to the

Graduate School-New Brunswick

Rutgers, The State University of New Jersey

In partial fulfillment of the requirements

For the degree of

Doctor of Philosophy

Graduate Program in Chemical & Biochemical Engineering

Written under the direction of

Ioannis P. Androulakis, PhD

Marianthi G. Ierapetritou, PhD

And approved by

_____

_____

_____

_____

New Brunswick, New Jersey

OCTOBER, 2010

ABSTRACT OF THE DISSERTATION

Development of Kinetic Model Reduction Framework and Its Application in Realistic Flow Simulation

By KAIYUAN HE

Dissertation Directors:

Ioannis P. Androulakis, PhD

Marianthi G. Ierapetritou, PhD

The main objective of this research is to develop a kinetic model reduction framework that enables incorporation of detailed chemistry with realistic flow simulation. Comprehensive computational fluid dynamics tools and detailed kinetic mechanisms have been developed, and the fully integration of these two components has been recognized as an imperative necessity to represent realistic systems. However, integrating detailed chemistry in complex flow simulation is expensive and oftentimes prohibitive. Thus this work is driven by the premise to reduce the computational intensity introduced by including detailed chemistry in realistic flow simulation and meanwhile retain acceptable accuracy. The work in this dissertation is focused on the development of an

efficient yet accurate kinetic reduction method that enables dynamic reduction within the context of reactive simulations.

Excessive computational intensity introduced by the integration of detailed chemistry in reactive flow simulation stems from the large size of detailed kinetic models. The kinetic model reduction method proposed in this dissertation is to address the following two unique aspects: (i) effective reduction of model size; and (ii) efficient integration of the reduction method dynamically during reactive flow simulation without introducing significant overhead. The proposed method is based on an element flux analysis approach which provides an indicator to quantify element transitions between species. The element flux can be further implemented to retrieve useful information from the kinetic network and identify active species under given reaction conditions, which constitute the fundamental of kinetic analysis and redundancy identification in mechanism reduction. It is demonstrated in this research that element flux analysis gives rise to both an effective and efficient dynamic mechanism reduction method, as well as a useful kinetic analysis tool. The proposed approaches can be extended to multiple disciplines since a large number of applications in novel fuel development, engine design, and petro chemistry require the efficient modeling of reactive flows.

ACKNOWLEDGMENTS

I would like to express my deepest gratitude to my thesis advisors Dr. Ioannis P. Androulakis and Dr. Marianthi G. Ierapetritou for their supervision, advice, and guidance during my PhD research. They not only educate me with necessary research techniques, but more importantly also teach me how to define a critical problem rather than solving a given one. Without their support and guidance much of the work presented in this dissertation would not have been possible. The high quality training I received from both of them has tremendously improved me as a junior researcher, and I believe it will continue benefit me in my future career. I am heartily thankful to them and I hope to have more opportunities to learn from them in the future.

I have been fortunate to collaborate with John T. Farrell, Sumathy Raman, and Long Liang at ExxonMobil. I would like to thank all of them for discussing with us their insightful comments on the technical details and direction of this research. Further, I would like to acknowledge Dr. Shapley for providing very insightful comments to my thesis proposal which greatly helped me to view problems in my research from different angles.

I would like to acknowledge the funding sources which supported me throughout my graduate student career and made this work possible. Support for this thesis has been provided primarily by the NSF CBET Grant 0730582, and ONR Contract N00014-06-10835. Additional support has been provided by ExxonMobil R&E Co.. Further, I would like to acknowledge the Androulakis group and the Ierapetritou group for their unconditional support during my graduate career.

Contents

List of Tables

List of Figures

Chapter 1

Introduction

1.1 Kinetic modeling of combustion process

The reaction engineering community has devoted significant research efforts towards the development of high-level detailed simulation schemes that accurately describe the physical transport and chemical reaction properties of complex reactive processes. Of particular importance is the analysis of combustion systems. This is due to the fact that approximately 85% of the energy consumed in the United States each year is generated from the combustion of fossil fuels, with transportation being a major contributor. Despite improvements, transportation-related combustion is responsible for significant amounts of NOx, CO, CO2, and other chemical species that are considered critical for air pollution and climate change. Advances in computational power offer an opportunity to improve our fundamental understanding of combustion at the molecular level so as to improve the energy use in transportation systems by improving kinetic models. Interactions between multiphase flow, complex chemical kinetics and hydrodynamic turbulence mixing all combine to characterize the combustion process.

The development of advanced reactive systems requires efficient and reliable models that provide full coupling of all relevant physical processes and chemistry. Although there is a dramatic increase in recent years in the use of comprehensive computational fluid dynamics tools to model combustion systems, most of the developed frameworks cannot afford the incorporation of detailed chemistry which has been recognized as an

imperative necessity to represent realistic systems. Incorporation of even skeletal kinetic mechanisms, e.g., less that 50 reacting species, increases significantly the computational effort as the solution of the reactive can account for over 90% of the CPU time. Our work in this project will focus on combustion systems although as it will be apparent in the following sections the tools that we propose can be extended to many processes.

To incorporate complex chemistry in comprehensive computational fluid dynamics tools, a number of detailed kinetic mechanisms have been developed to model a variety of chemical processes (Curran 1998; Faravelli, Antichi et al. 1997; Faravelli, Bua et al. 2001; Granata, Faravelli et al. 2002; Jiang, Qiu et al. 2005; Li and Williams 1999; Lindstedt 2003; Roesler, Yetter et al. 1995). However, detailed simulation of reactive flow systems using complex kinetic mechanisms consisting of hundreds of species and thousands of reactions is a computationally very demanding task. Hence considerable effort has been invested towards the representation of complex kinetic models by simpler, reduced, models which can largely alleviate the computational complexity while still retaining considerable accuracy (Androulakis 2000; Banerjee and Ierapetritou 2003; Bhattacharjee, Schwer et al. 2003; Griffiths 1995; J. Wei 1969; Peters 1988; Pope 1997; Turanyi 1990). Significant effort has therefore been invested in developing reduced representations of complex reaction mechanisms.

1.2 Reactive flow simulation

Reactive flows can be defined as fluid flows that are significantly affected by chemical reactions. The simulation of reactive flows requires advances in two areas: computational fluid dynamics (CFD) and detailed chemical kinetic modeling. As the increase of computational capability in recent years, more accurate computational fluid dynamics

(CFD) models have been developed. The fundamental basis of any CFD model is the solution of Navier-Stokes equations (Hirschfelder J.O. 1949). Further complicating factors are that the flow occurs in a complex geometry, the incorporation of turbulence, and the integration of detailed chemical kinetics. To describe turbulence several models have been developed such as direct numerical simulation (DNS) method (Reynolds 1989) and k-ε model (Jones 1985). In recent years much progress has been made in CFD model development for engines. For example, studies have been conducted for direct-injection diesel engines (Hou 1995; Patterson 1994), indirect-injection diesel engines (Scheimer 1995), stratified-charge rotary engines (Abraham 1989), and homogeneous-charge compression ignition engines (Aceves 2000; Babajimopoulos 2005). Although these engine simulation codes are comprehensive and can predict engine details to some extent, they are not entirely predictive for the combustion process due to the wide range of combustion time scales and engine conditions. Thus submodels have been developed to capture the short time scale processes such as drop vaporization (Chiang, Raju et al. 1992; Marchese, Dryer et al. 1999; Sirignano 1993) and turbulence dispersion (Mashayek 1998; Squires and Eaton 1991).

1.3 Integration of detailed chemistry in complex flow simulation

Sophisticated CFD models provide an accurate description of flow properties. However, the incorporation of CFD with detailed chemistry is computationally expensive, and often times prohibitive. Thus two broad categories of approximation approaches have been proposed to integrate CFD and detailed chemical kinetics: (a) detailed kinetic mechanisms coupled with simplified description of the flow field, and (b) detailed flow calculation coupled with simplified kinetic models.

In the engine simulation community, a number of approaches have centered on simplified flow calculations. This is usually achieved using the so-called “zone” approach. The earliest, and simplest example of this type of model were single-zone models (Najt 1983) which considered the entire engine reactor to be a single cell. Later, multi-zone models have been developed which divide the combustion chamber into multiple zones based on physical conditions (Babajimopoulos 2005).

Approximation approaches focusing on kinetic reduction encompass a multitude of techniques which generally fall in three categories: skeletal mechanism reduction, adaptive reduction, and on-the-fly reduction. Skeletal mechanism reduction approaches develop a global reduced mechanism to define the entire simulation. This category includes the redundant species identification and sensitivity analysis approaches proposed by Turanyi (Turanyi 1990) and Rabitz (Rabitz 1983), the quasi-steady-state-assumption (QSSA) and partial equilibrium approximations (Chen 1988; Peters 1988), the Intrinsic Low Dimensional Manifolds (ILDM) (Mass 1992), the Computational Singular Perturbation (CSP) (Lam 1994; Lu 2001), the direct-relation-graph (DRG) method (Lu 2005; Lu 2006a; Lu 2006b), the optimization-based mathematical programming approach (Androulakis 2000; Bhattacharjee, Schwer et al. 2003; Petzold 1999), and the element flux analysis based approach (Androulakis 2004b). However, a global mechanism cannot be always accurate for various conditions that are confronted in a reactive flow. Thus adaptive kinetic reduction strategy has been explored to use different mechanisms for different conditions. Several adaptive schemes have been proposed such as In Situ Adaptive Tabulations (ISAT) (Pope 1997), the “store and retrieve” approach (Androulakis 2004a), and reduction scheme subject to the validity of temperature, pressure, and species

compositions (Banerjee and Ierapetritou 2003; Schwer, Lu et al. 2003). In our work, an adaptive framework was developed based on flux graph analysis and clustering algorithms (He 2008). Adaptive reduction approaches are more accurate than global reduced mechanisms; however, they rely on the development of a library of reduced mechanisms which requires *apriori* analysis of the simulations. Due to the wide range of conditions encountered in chemical systems, the union of the feasible regions of reduced mechanisms in the library may not cover all possible reactive conditions. This deficiency has led some researchers to explore on-the-fly reduction methodologies which do not rely on priori analysis. The on-the-fly reduction schemes analyze local reactive conditions and dynamically develop reduced mechanisms which are locally accurate during the reactive flow simulation. Liang et al. (Liang 2008) proposed an on-the-fly approach based on the direct relation graph method (Lu 2005; Lu 2006a; Lu 2006b). In our work, an on-the-fly reduction scheme based on the element flux analysis was proposed. The element flux analysis was first introduced by Revel et al. (Revel, Boettner et al. 1994) and was implemented in mechanism reduction by Androulakis et al (Androulakis 2004b). The carbon flux between reacting species are calculated at each simulation time step and sorted in descending order. By setting a user-selected cutoff value, active species with large element flux can be identified, which constitute the local reduced mechanism to define the chemistry at this particular time step. No priori analysis or information is needed for this approach and the active species can be identified effectively without extensive computational overhead.

1.4 Motivation and outline of the dissertation

Mechanism reduction approaches introduced above predict the reaction system with high

fidelity comparing to the detailed mechanism. However, these approaches either lack the capability to derive different reduced mechanisms for different conditions, or are too expensive to be implemented *on-the-fly* in a realistic flow simulation. In order to arrive at a mechanism reduction approach that meets the requirements of both dynamic chemistry reduction and efficient on-the-fly implementation, we propose in this work a mechanism reduction approach based on element flux analysis. The proposed on-the-fly reduction framework does not depend on any apriori analysis or empirical knowledge. Locally accurate mechanisms are developed *on-the-fly* during the simulation based on instantaneous element flux which captures in a more sufficient way the local reactive propensity than T, P, and species concentrations. In the proposed methodology, the on-the-fly scheme develops reduced mechanisms based on the full array of species composition and system temperature and pressure, thus for any typical combustion simulations, using either 0-dimensional reactor model or a multi-dimensional CFD model, the reduction scheme can be integrated in the calculation with negligible computational overhead.

In this dissertation, the basic concepts and formulation of element flux analysis will be introduced first, followed by the description of mechanism reduction methods based on element flux analysis. Two reduction methods are presented in this dissertation, a graph-based adaptive reduction approach which employs a number of pre-developed reduced mechanisms to address different conditions in reactive flow simulations; and an on-the-fly reduction method which does not depend on any *apriori* analysis and develops a locally accurate mechanism dynamically within the context of simulations. Following the introduction of the methodology, the on-the-fly reduction method is demonstrated in

multi-dimensional CFD codes to fully integrate detailed chemistry and flow calculation. The element flux analysis has also been extended to multiple reaction networks such as NOx formation and soot formation in addition to hydrocarbon oxidation. A multi-element flux analysis approach is proposed to include all element transitions in combustion systems, and a graph searching technique is introduced to element flux analysis to separate reaction networks with different flux scales. Apart from mechanism reduction, element flux analysis also provides a metric to analyze the entire kinetic network and retrieve useful information from the kinetic mechanism, like connectivity between species, system evolution pathways, and other chemical characteristics. Thus in Chapter 5, a systematic kinetic analysis approach based on element flux is introduced. Finally, we demonstrate not only the potential implementations of the proposed kinetic mechanism reduction method and kinetic analysis tool, but also to advocate the possibility of the generalization of this framework in a wide range of chemical reaction systems and thus enabling the use of computational simulation to provide useful information for advanced chemical system design and novel fuel development.

Chapter 2

Dynamic Mechanism Reduction Based on Element Flux Analysis

2.1 Element flux analysis

The mechanism reduction methods presented in this dissertation are proposed based on element flux analysis. In our previous work (Androulakis 2000) we demonstrated how the concept of element flux analysis, first introduced by Revel et al.(1994), provides a pointer to quantify the activity of species in a reaction system. The instantaneous elemental flux of atom *A* from species *j* to species *k* through reaction *i*, denoted as $\dot{A}_{ijk}$, is defined in Eq.1. The total instantaneous flux between species *j* and *k* can be calculated by summing $\dot{A}_{ijk}$ over all the reactions in which species *j* and *k* are involved, as represented in Eq.2.

$$\dot{A}_{ijk}(t) = q_i(t)\frac{n_{A,j}n_{A,k}}{N_{A,i}} \tag{1}$$

$$\overline{\dot{A}}_{jk}(t) = \sum_{i=1}^{N_R} \dot{A}_{ijk}(t) \tag{2}$$

where $q_i(t)$ is instantaneous rate of reaction *i* (mol/s), $n_{A,j}$ is the number of atoms *A* in species *j*, $n_{A,k}$ is the number of atoms *A* in species *k*, $N_{A,i}$ is the total number of atoms *A* in reaction *i*, and N_R represents the number of reactions that these species participate as

reactants or products. However, we recently demonstrated (He 2008) that Eq.1 and Eq.2 do not properly represent element flux for quasi-steady-state species induced by partial equilibrium reactions. This is due to the small net reaction rates of partial equilibrium reactions compared to their respective forward and reverse reaction rates. Therefore, the flux pointer $\dot{A}_{ijk}$ calculated through Eq.1 is small although very fast element transition is taking place between species *j* and *k* through reaction *i*. To avoid underestimation of element flux for these quasi-steady-state species, both the forward and reverse reactions rates are taken into account in current work. Eq.1 has been modified as Eq.3:

$$\dot{A}_{ijk}(t) = (|q_{ifwd}(t)| + |q_{irev}(t)|)\frac{n_{A,j}n_{A,k}}{N_{A,i}} \tag{3}$$

where q_{ifwd} and q_{irev} are the reactions rates of forward and reverse reactions, respectively. The absolute values of both forward and reverse reaction rates can ensure no significant information loss when evaluating element flux for both partial equilibrium reactions and quasi-steady-state species.

2.2 Graph-based adaptive mechanism reduction

2.2.1 Adaptive mechanism reduction

To achieve an accurate simulation of reactive flows, it is recognized by researchers who intend to reduce detailed mechanisms that different mechanisms should be used for different conditions encountered in the simulation. That introduces the idea of adaptive reduction which employs a library of reduced mechanism with each of them addressing a certain range of conditions. In the adaptive reduction scheme, appropriate reduced mechanisms are selected to address different range of conditions through an effective

search algorithm during the simulation.

Most reduction schemes evaluate the appropriateness of a mechanism based on local temperature, pressure and composition characteristics. However, reaction systems at different temperature and compositions may activate the same pathways and reactions (Androulakis 2006). Element flux, introduced by Revel et al. (Revel, Boettner et al. 1994), allows one to capture the reactive propensity of the system more comprehensively. In our previous work, we extended this concept in order to develop time-integrated element flux graphs and explored their potential for mechanism reduction. Besides, we explored the hypothesis that the element flux graphs provide a better description of the reactive characteristics of the reaction mixture (Androulakis 2004b; Revel, Boettner et al. 1994). The flux graph analysis and mechanism reduction share some similar intrinsic characteristics: they both identify active species and reactions dominating the local reaction system at specific time point, which is the basis of the proposed reduction scheme. In (Androulakis 2004b; Revel, Boettner et al. 1994) it was shown that the reaction system under different conditions, as would be defined by species compositions, temperature, pressure, or sensitivities, may have the same reactive propensity which is directly represented by the chemical flux graph. Based on our prior work, we introduce in this work a new instantaneous flux graph method for analyzing and reducing complex kinetic mechanisms, and developing adaptively reduced representations. In the following sections, we illustrate this adaptive mechanism reduction approach using a detailed n-pentane oxidation mechanism including 385 species and 1895 reactions (Curran, Gaffuri et al. 1998).

2.2.2 Flux graph construction

Once the element flux between all source-sink pairs are calculated in Eq.2 and Eq.3, we have a list of fluxes and corresponding source species and sink species. This provides information about the existence of connectivity between two species as well as the strength of the connectivity (flux value), as shown in Table 2.1. Based on this flux list, a flux graph can be constructed by considering species as graph nodes and weighing graph edges proportional to the flux between two species. In the present work, carbon-atom flux is analyzed to identify active species that describe major carbon pathways. However, species that are crucial to H/O chemistry are also included in the mechanism to describe the H/O chemistry as well as the carbon chemistry. Graph visualization software GRAPHVIZ (Gansner, Koutsofios et al. 2006) is used in this work as a drawing tool to construct flux graphs. An example of flux graph illustrating n-pentane oxidation is shown in Figure 2.1. The entire graph consists of 385 nodes and 1954 edges. For illustration purpose, only the most important species transitions are shown in the flux graph.

Table 2.1: Instantaneous element fluxes of initial stage of n-pentane oxidation in a plug-flow reactor (PFR) model. Initial temperature: 700K; fuel equivalence ratio: 1.0.

Index	Sources	Sinks	Instantaneous Carbon Flux	Cumulative Flux Sum	Cumulative Weight
1	NC5H12	C5H11-2	28.828	28.828	11.86%
2	C5H11-2	C3H6	15.793	44.621	18.36%
3	NC5H12	C5H11-3	14.371	58.992	24.27%
4	NC5H12	C5H11-1	14.367	73.359	30.18%
5	C5H11-2	C2H5	10.528	83.887	34.51%
6	C2H5	C2H4	7.314	91.201	37.52%
7	C5H11-3	C5H11O2-3	6.949	98.150	40.38%
8	C5H11-3	C4H8-1	6.035	104.185	42.87%
9	C5H11-1	C5H11O2-1	5.763	109.948	45.24%
10	C5H11O2-3	C5H10OOH3-2	4.993	114.941	47.29%
11	C5H10OOH3-2	C5H10-2	4.924	119.866	49.32%
12	C3H6	IC3H7	4.582	124.447	51.20%
13	C5H11-1	NC3H7	4.376	128.823	53.00%
14	C5H11-2	C5H11O2-2	4.164	132.987	54.72%
15	HCO	CO	3.404	136.391	56.12%
16	C5H11-1	C2H4	2.917	139.308	57.32%
17	CH3O	CH2O	2.907	142.215	58.51%
18	C5H11O2-1	C5H10OOH1-3	2.619	144.834	59.59%
19	C2H5	C2H5O	2.582	147.416	60.65%
20	C5H11O2-2	C5H10OOH2-4	2.416	149.833	61.65%
21	C5H10-2	C5H9	2.237	152.069	62.57%
22	IC3H7	IC3H7O2	2.188	154.258	63.47%
23	NC3H7	NC3H7O2	2.104	156.362	64.33%
24	CH2O	HCO	2.062	158.424	65.18%
25	C3H6	C3H5-A	2.056	160.479	66.03%
26	C2H5	C2H5O2	2.007	162.486	66.85%
27	C5H10OOH1-3	C5H10O1-3	1.971	164.457	67.66%
			⋮		
			Total Flux	**243.053**	

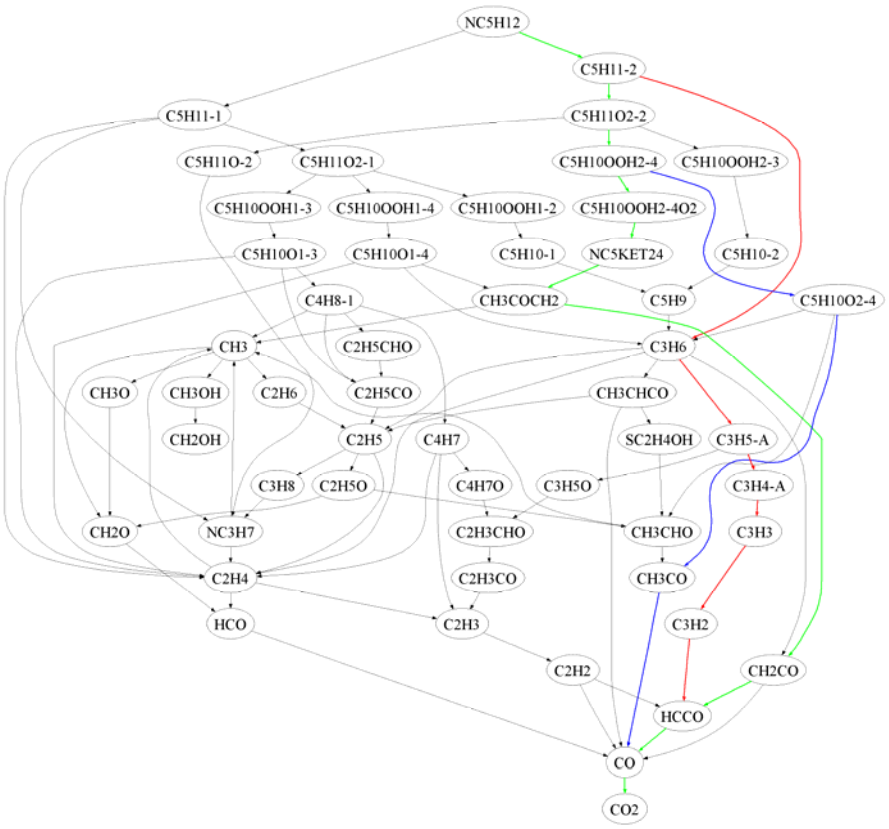

Figure 2.1: Flux graph of n-pentane oxidation. Highlighted pathways shows active pathways under different temperatures. Red: high temperature pathway; blue: medium temperature pathway; green: low temperature pathway.

2.2.3 Graph clustering

Once the flux graph has been derived, it is monitored in a dynamic way as the reaction system evolves. A snapshot of the reaction system is obtained at every time step which corresponds to a unique flux graph with the same structure as shown in Figure 2.1, but with different edge weights (flux values). Since this graph-based adaptive reduction approach attempts to capture the reaction propensity of the mixture through the use of flux graphs, and bases its mechanism reduction rationale on the hypothesis that similar flux graphs are associated with similar reaction mechanisms, it becomes important to be able to quickly and accurately compare and cluster the graphs emanating from different conditions during the simulation.

In order to identify similar snapshots and group them into clusters to represent different stages of the reaction progress, a graph comparison technique and clustering algorithm, along with a search method are needed. In brief, a clustering algorithm involves the following components: a set of objects, such as graphs in our work; a measure to assess similarity (or dissimilarity or distance) between pairs of objects; and a clustering method that identifies groups of both internally homogeneous and externally distinct based on the similarity data.

In this work, given the large number of nodes and edges included in the flux graph, each instantaneous flux graph is considered as an N dimensional vector, where N stands for the total number of reactive fluxes in the system. In doing so element flux graphs captured under different circumstances are treated as multi-dimensional vectors with the same number of dimensions but different values for each dimension. The vector is monitored over time and compared in order to assess similarities between corresponding graphs, which will denote similarities in the underlying chemistry. Representing a flux graph G by a vector V we quantify the similarity between flux graphs by evaluating the distance between corresponding vectors using either cosine coefficient (Schultz and Liberman 1999) or normalized 1^{st} order Minkowski distance. The cosine coefficient calculates the cosine of the angle between two vectors and considers the angle as an indication of vector similarity. The 1^{st} order Minkowski distance evaluates distance between two vectors by summing up the difference between the values for each dimension of the vectors.

In this adaptive reduction approach, the first stage is to build up a library of reduced mechanisms with each covering different conditions. Since these reduced mechanisms are developed based on flux graphs sampled during simulations under different conditions, as

described in details in the following section, a large training set of flux graphs covering a wide range of condition space is needed. Therefore, n-pentane oxidation process is simulated using an adiabatic plug-flow reactor (PFR) model under initial temperature ranging from 600 K - 1100 K and fuel equivalence ratio ranging from 0.5 to 2.0. The training data set consists of 47189 instantaneous flux graphs, which are perceived as a data set of 47189 1954-dimensional vectors (correspond to 1954 edges in the flux graph). Based on the data set, hierarchical clustering algorithm is used to obtain k-way clustering, where k represents the number of clusters to be exported in the clustering process. To implement hierarchical clustering, first we need to define the distance (or similarity) coefficients to be used to assess the distance (or similarity) among vectors. Two coefficients are employed in this work, one is cosine coefficient as defined in Eq.4, and the other is normalized 1-norm distance (Minkowski distance of order 1) as defined in Eq.5, ordinary 1-norm distance is also presented as Eq.7:

$$S_{AB} = \frac{\sum_{j=1}^{j=n} x_{jA} x_{jB}}{[\sum_{j=1}^{j=n} (x_{jA})^2 \sum_{j=1}^{j=n} (x_{jB})^2]^{1/2}} \tag{4}$$

$$D_{AB} = \sum_{j=1}^{j=n} \left| \frac{x_{jA}}{\sum_{i=1}^{i=n} x_{iA}} - \frac{x_{jB}}{\sum_{i=1}^{i=n} x_{iB}} \right| \tag{5}$$

where x_{jA} and x_{jB} express for value of *jth* element of vector A and B, respectively; *n* is the dimension of the vector. The cosine coefficient (Eq.4) evaluates similarity among multi-dimensional vectors while the normalized 1st order Minkowski distance (Eq.5) indicates distance among vectors.

Given the distance matrix (or similarity matrix), a clustering algorithm is implemented to

group similar flux graphs into clusters. A hierarchic agglomerative approach (Jardine 1968) is employed in this work, which merges pairs of objects that are most similar into a cluster and consider this cluster as a single object in the following iteration. This step is repeated and hierarchies are built up by progressively merging clusters. Another commonly used clustering algorithm is k-means algorithm (Kanungo, Mount et al. 2002). The algorithm uses an iterative refinement starts by partitioning the objects in the dataset into k initial sets, either at random or using some heuristic data. It then calculates the mean point, or centroid, of each set and constructs a new partition by associating each point with the closest centroid. Then the centroids are recalculated for the new clusters, and the algorithm continuously alternates these two steps until the centroids are no longer changed. The hierarchical clustering algorithm is performed using the CLUTO package (Karypis 2002). Both cosine coefficients and normalized 1^{st} order Minkowski distance function were implemented in this work and similar results were obtained. Since the cosine coefficient is optimized in CLUTO based on its properties, the remaining part of the methodology and results are presented using cosine coefficient.

In the clustering step, a 30-way cluster is employed which maximizes intra-cluster similarity while minimizes inter-cluster similarity. The outcome of this step is 30 clusters, each containing a certain number of flux graphs from the training set. These 30 clusters cover different range of reaction conditions. As shown in Figure 2.2, each cluster covers a different range of n-pentane mass fraction and temperature. Six typical clusters are selected and their coverage is shown in Figure 2.3.

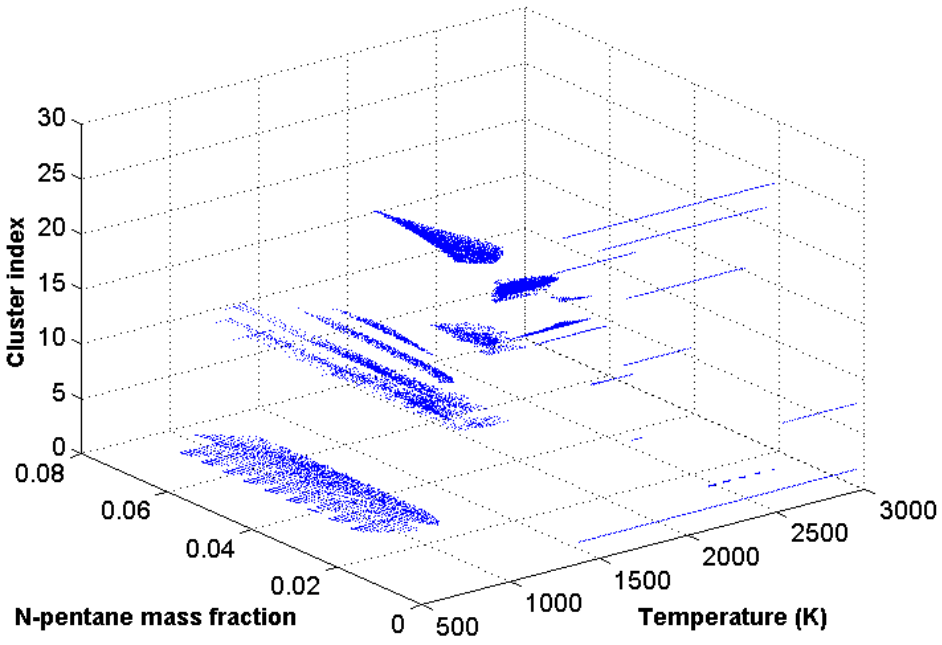

Figure 2.2: Temperature and pentane mass fraction range covered by each cluster in the 30-way clustering.

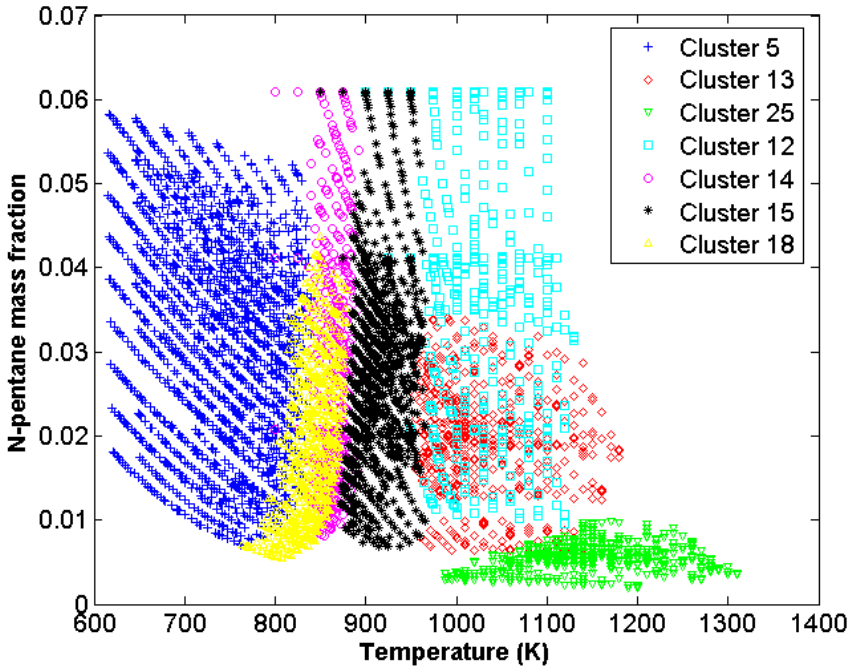

Figure 2.3: Temperature and pentane mass fraction range covered by clusters 5, 13, 25, 12, 14, 15, and 18 in the 30-way clustering.

2.2.4 Development of reduced mechanism library

After the clusters are generated to represent the dataset and the search method is defined, we need to assign each cluster a reduced mechanism. The purpose is to establish a library of reduced mechanisms that are linked to each cluster and can best characterize the reactive propensity of the cluster.

To identify species to be included in each reduced mechanism, for each flux graph in a cluster fluxes are sorted in a descending order and a high percent cutoff is applied. Species above the cutoff which correspond to large flux are considered to be important while species below the cutoff are considered to be trivial. This sort-and-cut procedure is done for every flux graph in each cluster. Then the union set of active species from all graphs in each cluster is used to define the reduced mechanism for this cluster. The sizes of reduced mechanisms developed by setting a 99% cutoff are listed in Table 2.2.

Table 2.2: Reduced mechanism size for n-pentane oxidation generated in the 30-way clustering and 99% cutoff in the mechanism development.

Mechanism	Species	Reactions	Mechanism	Species	Reactions
1	33	137	16	96	651
2	65	338	17	73	480
3	124	520	18	150	803
4	56	279	19	145	809
5	139	640	20	147	941
6	58	311	21	105	687
7	69	410	22	115	755
8	22	63	23	65	422
9	61	345	24	106	729
10	80	526	25	142	911
11	49	238	26	132	816
12	137	740	27	86	576
13	151	968	28	66	421
14	143	760	29	151	843
15	143	768	30	67	417
Average size	99.2	576.8			
Detailed	385	1895			

2.2.5 Search algorithm during simulations

The result of this first stage is the construction of a library of clusters and corresponding reduced mechanisms that can predict the reactive propensity of each cluster. The next step, in order to develop the adaptive chemistry representation, is to define a search algorithm that will assign a new query point to a particular cluster and subsequently the reduced mechanism associated with this cluster. In this work, we introduce a search algorithm with similar rationale to the Nearest-Neighbor (N-N) Search (Arya, Mount et al. 1998). N-N algorithm searches the object in the dataset that is nearest to a new query object, and the new object is classified to the category of this nearest neighbor. In this adaptive reduction approach, instead of searching among all the data points in the training set to find the nearest neighbor, it is only necessary to search among cluster centers, which is the mean vector of all the vectors in each cluster. As introduced above, 30 clusters are generated and therefore, 30 cluster centers are used to represent the corresponding clusters. During the simulation, the flux graph is evaluated at each time step and its distances to all the 30 cluster centers are calculated. The cluster with its center closest to the new query point is used to represent the current condition and its associated reduced mechanism is used to define the local chemistry.

2.2.6 Demonstration of the proposed adaptive framework

The proposed methodology is demonstrated in a Pair-wised Mixing Stirred Reactor (PMSR) model (Pope 1997) and a Plug-Flow Reactor (PFR) model for n-pentane combustion.

A pair-wise mixing stirred reactor (PMSR) model is used first to validate the reduced mechanisms and search algorithm in this work. In a PMSR model reactive fluid

composed of fuels, oxidizers, and diluents is modeled as even number of particles. The simulation is advanced in discrete time steps. Between these time steps, these particles are arranged in pairs and the composition of each particle undergoes a mixing-and-reaction evolution pattern, which means the composition first evolves through a mixing fractional time step and a reaction fractional time step afterward. The microscale mixing of each pair of particles (say, p and q) is described by Eq.6:

$$\frac{d\varphi^{(p)}}{dt} = -(\varphi^{(p)} - \varphi^{(q)}) / \tau_{mix}$$

$$\frac{d\varphi^{(q)}}{dt} = -(\varphi^{(q)} - \varphi^{(p)}) / \tau_{mix} \tag{6}$$

where τ_{mix} is the mixing timescale, $\varphi^{(p)}$ and $\varphi^{(q)}$ are compositions of particle p and q, respectively.

The PMSR simulation is performed with 100 particles and 100 steps, and the time step is $\Delta t = 3.1e10^{-3}$ s. The mixing time scale is $\tau_{mix} = 3.1e10^{-2}$ s, the paring time scale is $\tau_{paring} = 3.1e10^{-2}$ s, and the residence time scale is $\tau_{res} = 3.1e10^{-1}$ s. 30 reduced mechanisms developed in previous section are used in the simulation. Temperature and selected species profiles are compared in Figure 2.4. Due to the stochastic nature of the PMSR model, the average results of 3 simulations are used in Figure 2.4. An average error of 0.035 for temperature and selected species profiles was observed. While high level of accuracy is retained in the adaptive scheme, CPU time is tremendously reduced.

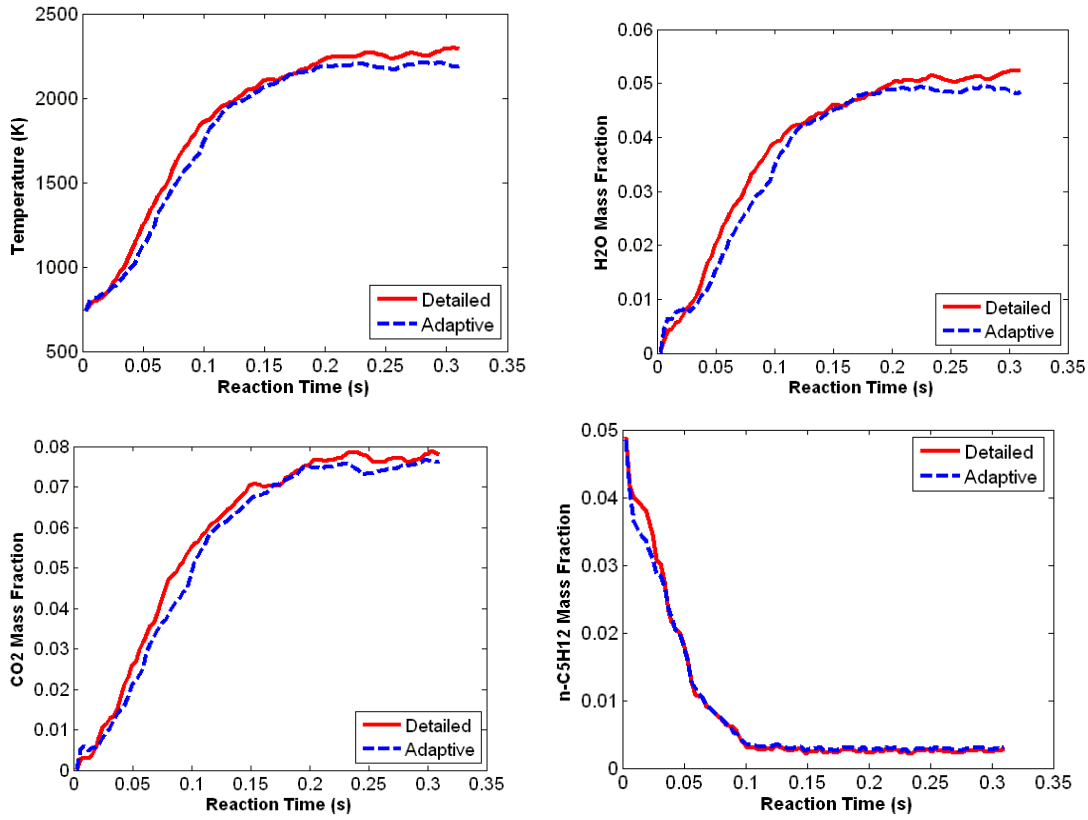

Figure 2.4: Performance of adaptive scheme in the prediction of temperature and composition profiles for 740K, Φ=1.0 in a PMSR.

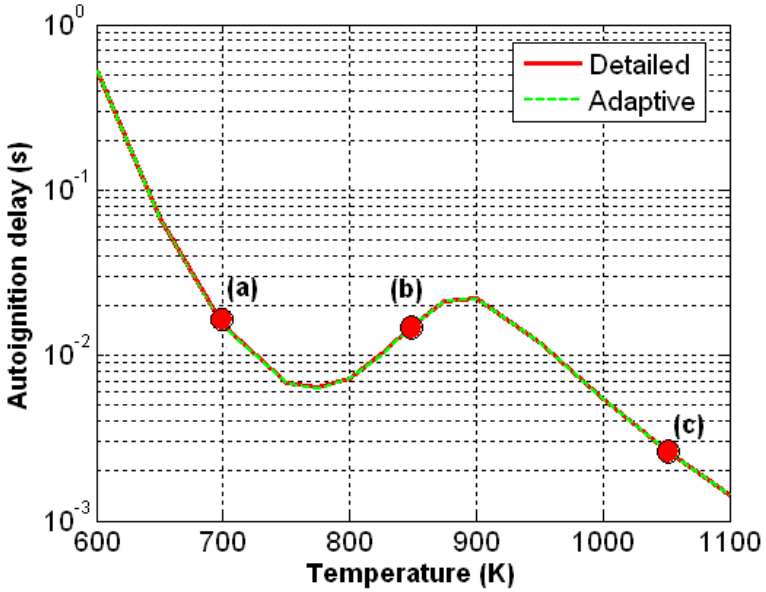

Figure 2.5: Autoignition delay times of n-pentane combustion predicted by adaptive scheme and detailed simulation.

The adaptive scheme is also tested in an adiabatic Plug-flow reactor (PFR) model to illustrate the performance of the adaptive scheme in the prediction of autoignition delay of n-pentane oxidation. The autoignition delays predicted by the adaptive scheme are calculated from different initial temperatures using stoichiometric ratio. The initial temperatures range from 600K to 1100K, which cover the low temperature, NTC temperature and high temperature oxidations. The autoignition delays predicted by the adaptive scheme are compared with those predicted by the detailed mechanism in Figure 2.5. Excellent agreement can be observed between two profiles, indicating that the proposed adaptive approach can accurately predict the autoignition delay time of n-pentane combustion under a wide range of temperature.

2.3 On-the-fly mechanism reduction

The adaptive reduction approach introduced in the previous section effectively reduced the mechanism size and retained good accuracy. However, the adaptive approach relies on the development of a library of reduced mechanisms before it cab be implemented in reactive simulations. Furthermore, the adaptive approach is based on the assumption that reduced mechanisms in the library can cover the entire condition space, which is usually not the case. When some rare conditions are confronted in a reaction system, which are not covered by the feasible regions of reduced mechanisms, the library becomes insufficient. Sensing this, in our later work we proposed an on-the-fly reduction scheme that dynamically identifies reduced mechanism for local conditions in the reaction process. The mechanism reduction method employs similar rationale to the adaptive approach: large element fluxes involve important species. To achieve on-the-fly reduction, the element fluxes between sources and sinks are calculated at each simulation time step

and sorted in descending order. By setting a user-selected cutoff value, active species correspond to large element fluxes are identified and used to define local chemistry. The CHEMKIN package(Kee 1996), which is used in the current flow model to compute chemistry, is employed in the reactive flow simulation to generate a reduced mechanism *on-the-fly* based on the identified species set. The main advantages of this approach are (a) no *apriori* analysis or information is needed, and thus the approach can be applied to any reactive conditions encountered in the reactive flow simulation; and (b) the active species can be identified effectively without extensive computational overhead. The on-the-fly reduction framework is summarized in Figure 2.6.

To validate the feasibility and accuracy of the on-the-fly reduction approach, the reduction scheme is demonstrated in the context of the same reactor models used in previous sections: PMSR and PFR. The same models are used primarily because they are computational tractable even with detailed kinetic model, and covers a broad range of conditions in the composition space. These properties merit our research in two aspects, (a) the reactive flow simulation in both models can be solved with detailed kinetic mechanism to provide temperature and composition profiles which are used to evaluate the performance of the on-the-fly reduction scheme; and (b) the PFR predicts autoignition delay which is considered as an important property of fuels and the stochastic pairing process in PMSR provides a wide range of reactive conditions to validate the on-the-fly reduction scheme.

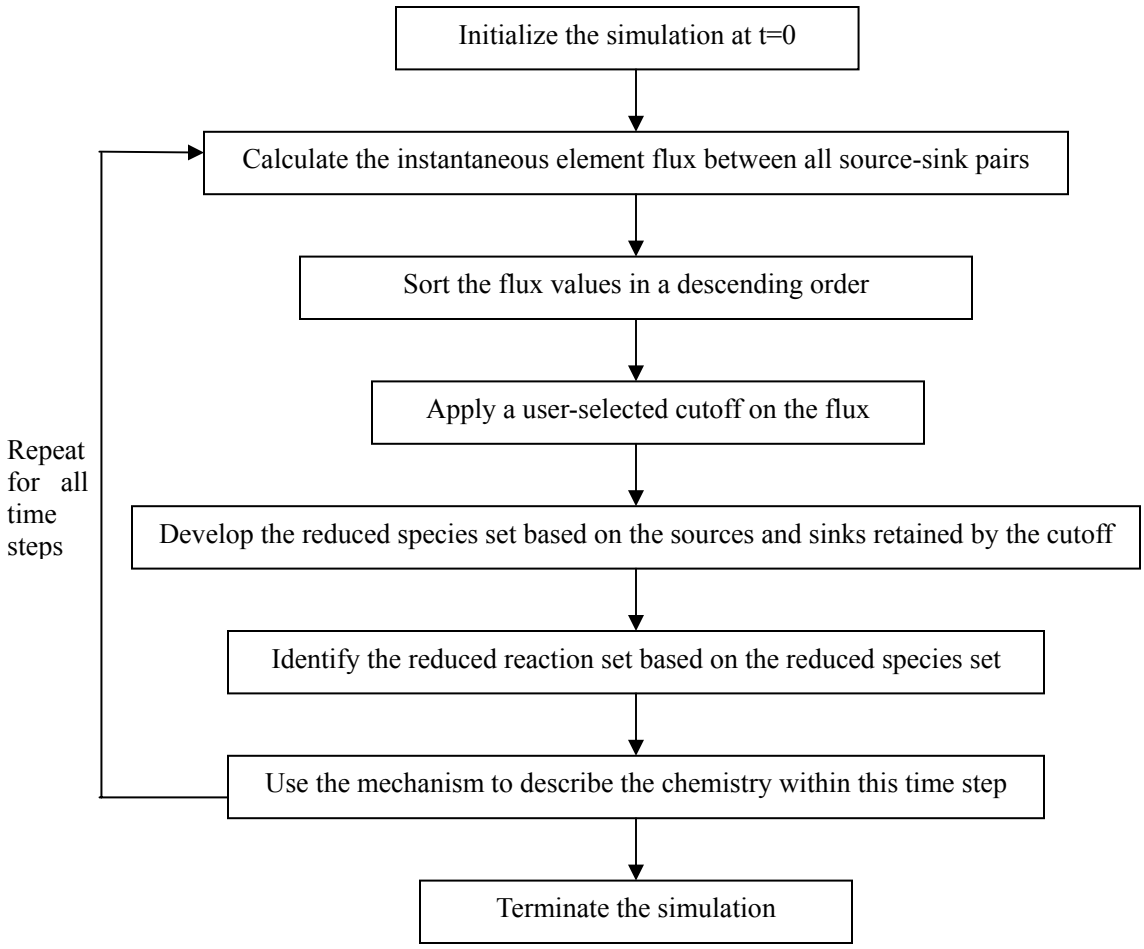

Figure 2.6: Integration of the on-the-fly reduction scheme in the context of a reactor model.

A detailed mechanism for Primary Reference Fuels (PRF) (Curran 1998) is used in the demonstration. The PRF, the mixture of n-heptane and iso-octane, is used to define the octane number for gasoline. Octane number (ON) is the number which gives the volume percentage of iso-octane in a mixture of iso-octane and n-heptane, which would have the same anti-knocking capacity as the fully blended gasoline under consideration. The detailed mechanism consists of 1034 species and 4236 reactions, which provides a good benchmark to demonstrate the capability of the proposed on-the-fly reduction in addressing large kinetic mechanisms. In the PMSR test, a 99% cutoff is used for the

on-the-fly reduction scheme and the results are shown in Figure 2.7. Excellent agreement was observed between the results predicted by the on-the-fly reduction scheme and those obtained with the detailed mechanism. The 99% cutoff used in the on-the-fly reduction scheme yields an average error of 4.6% while the CPU time was reduced by a factor of 40.

The on-the-fly reduction method is also tested in a PFR model using the primary reference fuel mechanism to predict the autoignition delays in the shock-tube experiments of Fieweger et al. (Fieweger 1997). Different octane numbers (ON=0, ON=80, ON=100) are tested in the simulations and the results are plotted in Figure 2.8. Good agreement was observed between predicted and experimental autoignition delay times for pure n-heptane (ON0), ON80 mixture, and pure iso-octane (ON100). The negative temperature coefficient (NTC) regions are well simulated by the detailed mechanism and on-the-fly reduction scheme. As the ON increases, which means the volume fraction of less reactive iso-octane increases, greater autoignition delay times of PRF mixture can be observed in both the experimental and simulated results.

2.4 Summary

Element flux analysis is introduced to describe the reaction system and develop mechanism reduction methods. The adaptive reduction approach employs a novel graph-based technique to develop representative reduced mechanisms and assign appropriate mechanism to given reaction conditions. By applying the flux analysis dynamically during the simulation, an on-the-fly reduction method is proposed which does not depend on any *apriori* analysis. At each time step of the computation, a reduced mechanism is generated based on local conditions and no previous information or

analysis is necessary.

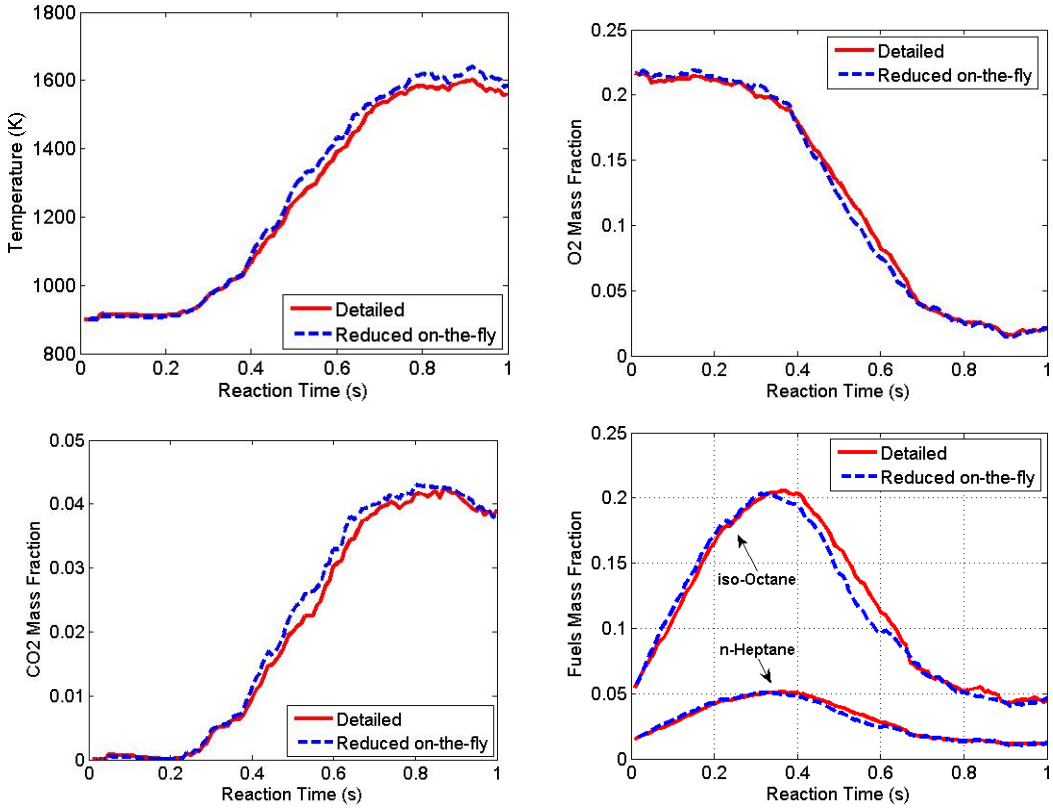

Figure 2.7: On-the-fly scheme tested for PRF oxidation in PMSR. Initial conditions: T=900K, ON=80, $y_{iso\text{-}octane}$=0.050, $y_{n\text{-}heptane}$=0.012, y_{O2}=0.219, y_{N2}=0.719.

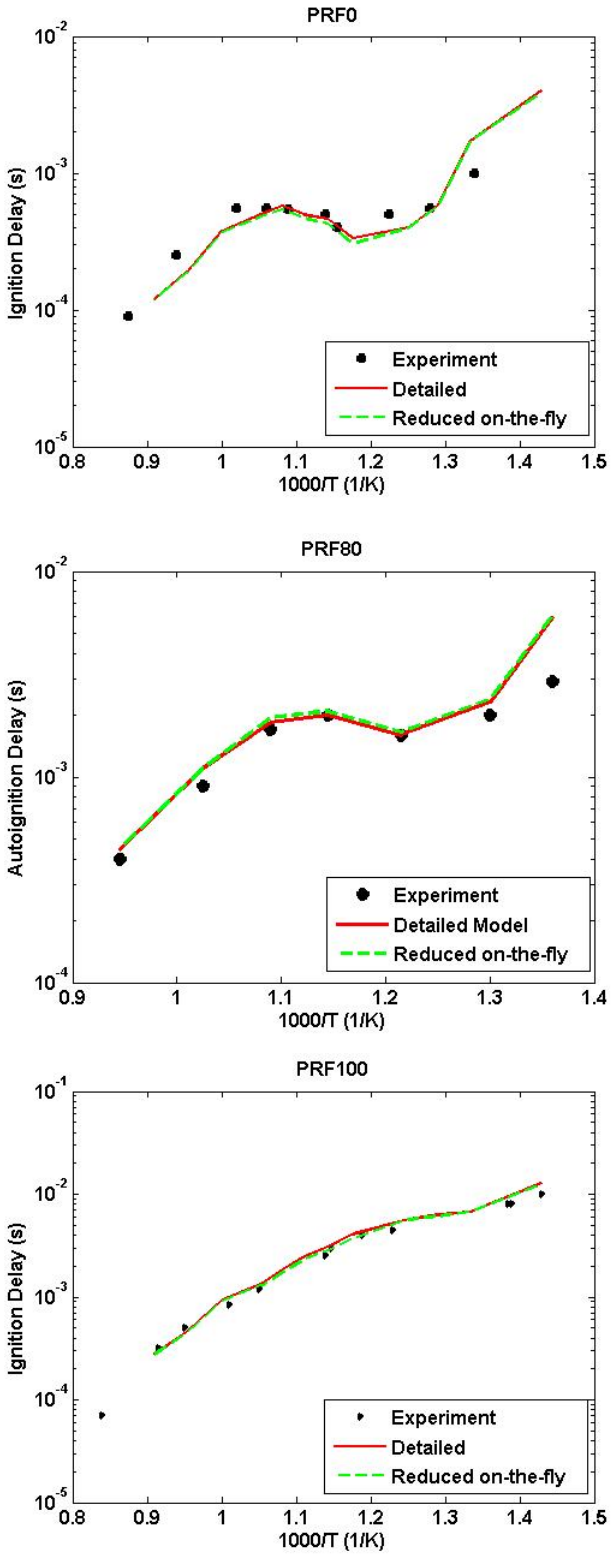

Figure 2.8: Autoignition delay times of primary reference fuels with different octane numbers at 40atm, stoichiometric fuel in shock-tube experiments versus model simulation. Experimental data from Fieweger 1997.

Chapter 3

Incorporation of Detailed Chemistry in Reactive Flow Simulations Using On-the-fly Reduction

3.1 Demonstration of the on-the-fly reduction in CFD

3.1.1 CFD model

In the previous Chapter, an on-the-fly reduction scheme was proposed to develop reduced mechanisms dynamically in reactive simulations. Reactor models with simple geometry have been used to validate the on-the-fly reduction methodology and good agreement was observed between the on-the-fly scheme and simulations using detailed mechanism. To further validate the reduction scheme, it needs to be integrated in a multi-dimensional CFD model which simulates fuel combustion in realistic engines.

In this Chapter, the on-the-fly reduction scheme is integrated in the framework of an engine CFD KIVA-3V (Amsden 1997) using a 2D numerical mesh with moving boundaries to simulate homogeneous charge compression ignition (HCCI) combustion. In the present study, KIVA-3V code has been selected as the engine model since it is a well developed package with the ability to calculate three-dimensional flows in engine cylinders, arbitrary piston shapes, effects of turbulence, and heat gradients near walls. The more essential factor is that the source code of KIVA is accessible and thus it can be used in model development work where KIVA serves as a test bed. The major reason we chose to use the on-the-fly reduction method in KIVA-3V to simulate HCCI combustion

is that HCCI combustion is mostly governed by kinetics, which provides a good test bed to demonstrate the proposed method in addressing complex kinetics in a CFD simulation. The governing equations of fluid dynamics and chemical kinetics in KIVA-3V are summarized below:

The continuity equation for species m is

$$\frac{\partial \rho_m}{\partial t} + \nabla \cdot (\rho_m \mathbf{u}) = \nabla \cdot [\rho D \nabla (\frac{\rho_m}{\rho})] + \dot{\rho}_m^c + \dot{\rho}^\delta \tag{3.1}$$

where ρ_m is the mass density of species m, ρ is the total mass density, and **u** the fluid velocity. $\dot{\rho}_m^c$ and $\dot{\rho}^\delta$ are source terms due to chemistry and the spray, respectively. In a HCCI simulation, the spray term is absent.

The momentum equation for the fluid mixture is

$$\frac{\partial (\rho \mathbf{u})}{\partial t} + \nabla \cdot (\rho \mathbf{u}\mathbf{u}) = -\nabla p - A_0 \nabla (2/3 \rho k) + \nabla \cdot \boldsymbol{\sigma} + \mathbf{F}^S + \rho \mathbf{g} \tag{3.2}$$

where p is the fluid pressure. A_0 is zero in laminar calculations and unity when turbulent models are used. In the present study of HCCI engine combustion which is dominated by chemical kinetics, A_0 is set as zero and thus the second term of the RHS is neglected.

The internal energy equation is

$$\frac{\partial (\rho I)}{\partial t} + \nabla \cdot (\rho \mathbf{u} I) = -p \nabla \cdot \mathbf{u} + (1 - A_0) \boldsymbol{\sigma} : \nabla \mathbf{u} - \nabla \cdot \mathbf{J} + A_0 \rho \varepsilon + \dot{Q}^c + \dot{Q}^s \tag{3.3}$$

where I is the specific internal energy, exclusive of chemical energy. $\dot{Q}^c$ and $\dot{Q}^s$ are the source terms due to chemical heat release and spray interactions. In HCCI simulation, the source term $\dot{Q}^s$ due to spray is zero.

3.1.2 Validation of the on-the-fly reduction method in CFD

To validate the proposed on-the-fly reduction scheme, the detailed n-pentane oxidization mechanism consists of 385 species and 1895 reactions (Curran, Gaffuri et al. 1998) is used in KIVA-3V. KIVA-3V handles the fluid mechanical processes on a highly resolved mesh grid. For 2-D simulation of HCCI engines, the challenge for mesh generation is its geometry complexity and moving piston and valves. Since the HCCI engine combustion is mainly controlled by chemical kinetics, only the temperature gradient near the engine walls and pistons are taken into account in the present study. In order to provide high enough resolution to describe the geometry of the HCCI engine and meanwhile keep the computation task accessible to current computers, a 2-D numerical mesh which has approximately 1000 cells at bottom dead center (BDC) position is generated for the simulation, as shown in Figure 3.1.

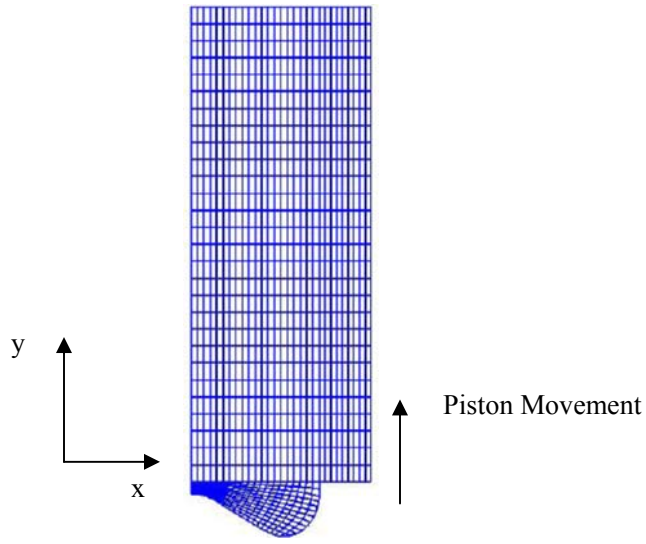

Figure 3.1: Numerical mesh of KIVA-3V used in current study.

KIVA-3V simulations are monitored from -40° to 30° after top dead center (ATDC). System temperatures at -40° ATDC are chosen as 725K, 820K, and 1000K to represent low, intermediate, and high temperature combustion, respectively. Typical HCCI operations starting from -180° ATDC at 300K to 450K will heat the cylinder to the range of 700K to 900K when piston reaches -40° ATDC (Kong and Reitz 2003b; Kong and Reitz 2003a). The simulations in this work were monitored from -40° ATDC to 30° ATDC because the major part of combustion occurs in this range and simulations of the full compression process (from -180° ATDC to 180° ATDC) would require substantially more CPU time. Detailed engine parameters and run conditions are listed in Table 3.1.

Table 3.1: Engine parameters and operating conditions of KIVA-3V simulations.

Parameter	**Value**
Engine speed	700 rpm
Compression ratio	16:1
Fuel	n-pentane
Start of calculation	-40
Initial pressure	5 bar
Equivalence ratio	1.0

Results of the on-the-fly scheme have been compared with simulations using the detailed mechanism. The detailed mechanism consists of 385 species and 1895 elementary reactions. The average size of reduced mechanisms generated in the on-the-fly reduction is 82 species and 451 elementary reactions. Figures 3.2 - 3.4 illustrate pressure and temperature profiles of HCCI operations under 725K, 820K, and 1000K at -40° ATDC, respectively. As shown in the pressure and temperature profiles, both the ignition timing

and the peak pressure are well predicted by the on-the-fly scheme. Since on-the-fly scheme dynamically develops accurate mechanisms for local conditions, at each time step a small mechanism is capable to capture most of the reactive propensity of the system. Thus although the average size of mechanisms in the on-the-fly simulation are small compared to the detailed mechanism, excellent accuracy can be achieved.

Concentration histories of fuel, oxidizer, OH radical, and product H_2O are compared with detailed simulation in Figure 3.5, which also showed encouraging agreement and further validated the effectiveness of the on-the-fly scheme. CPU times for the on-the-fly reduction scheme and the detailed simulation are compared in Figure 3.6. Three factors are represented in the figure: (1) the overhead introduced by the flux analysis and mechanism reduction; (2) CPU time for chemical kinetics calculation; and (3) CPU time for flow calculation. As we can see from the detailed simulation, more than 90% of the total CPU time was spent on resolving the chemistry part. Using the on-the-fly simulation, the CPU time spent for the chemistry part was significantly reduced while flow calculation was comparable with the detailed simulation. The overhead introduced by the flux analysis and mechanism reduction comprises less than 5% of the total CPU time of the on-the-fly simulation. By comparing the CPU times on all these parts, the on-the-fly scheme reduced the chemistry calculation by a factor of 30 and the overall CPU time by a factor of 20.

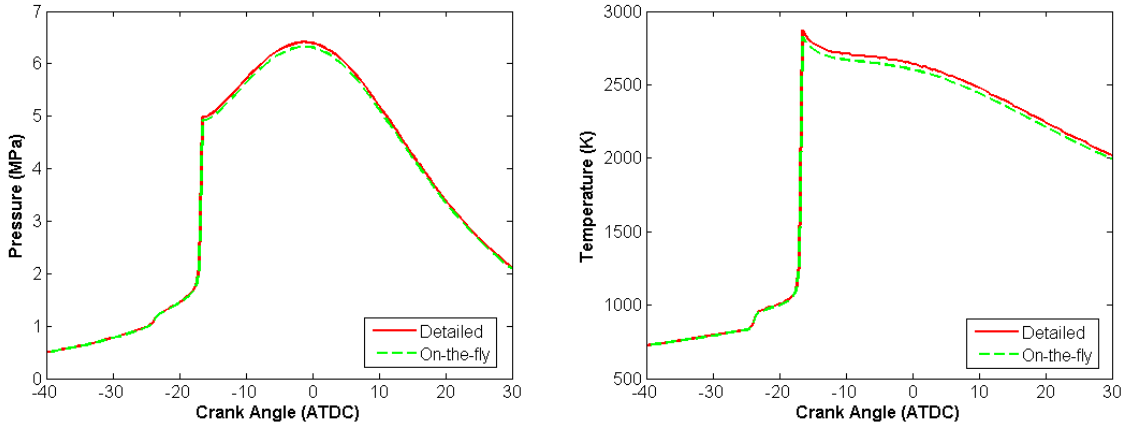

Figure 3.2: In-cylinder pressure and temperature profiles of n-pentane combustion in KIVA at 725 K and 5 bar.

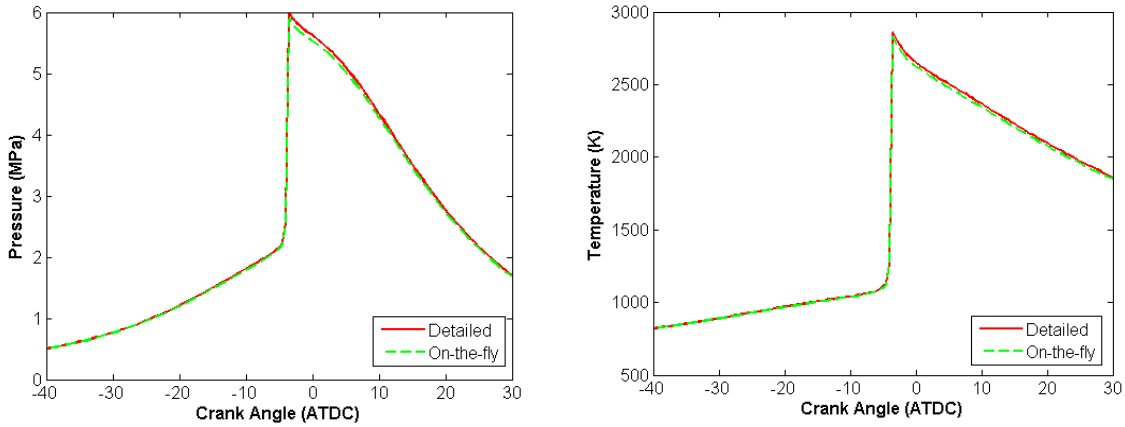

Figure 3.3: In-cylinder pressure and temperature profiles of n-pentane combustion in KIVA at 820 K and 5 bar.

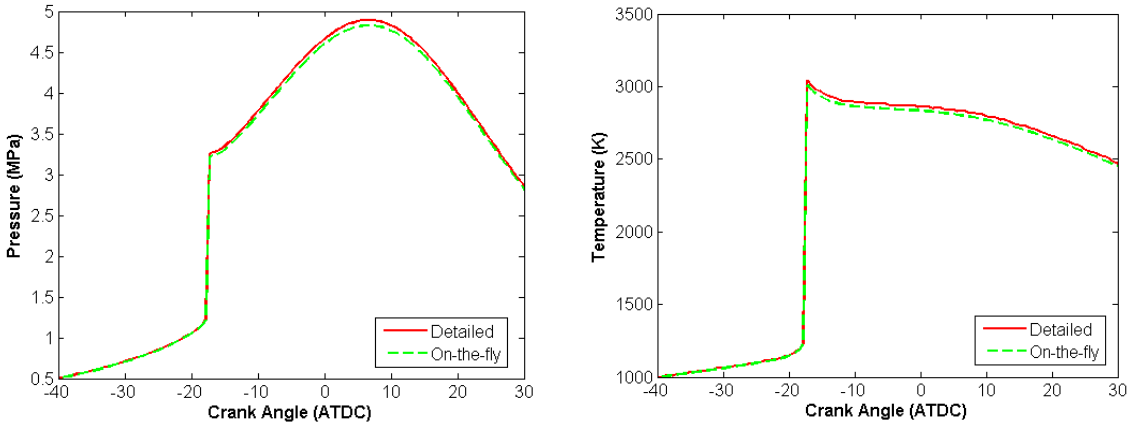

Figure 3.4: In-cylinder pressure and temperature profiles of n-pentane combustion in KIVA at 1000 K and 5 bar.

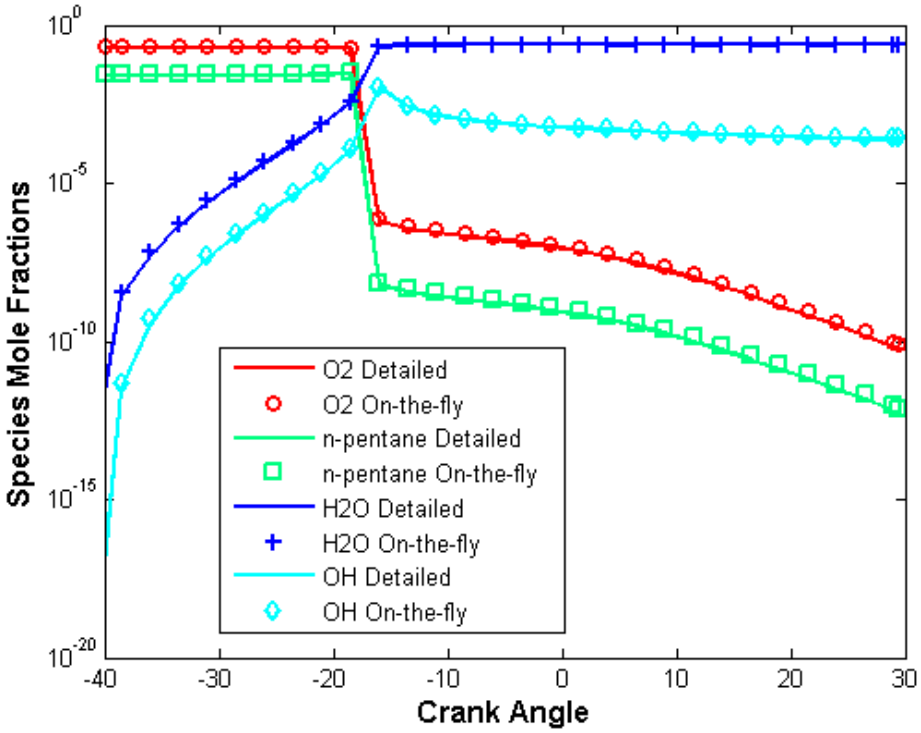

Figure 3.5: Species mass fractions of n-pentane combustion in KIVA at 1000 K and 5 bar. Lines represent the detailed simulation and markers represent the on-the-fly simulation.

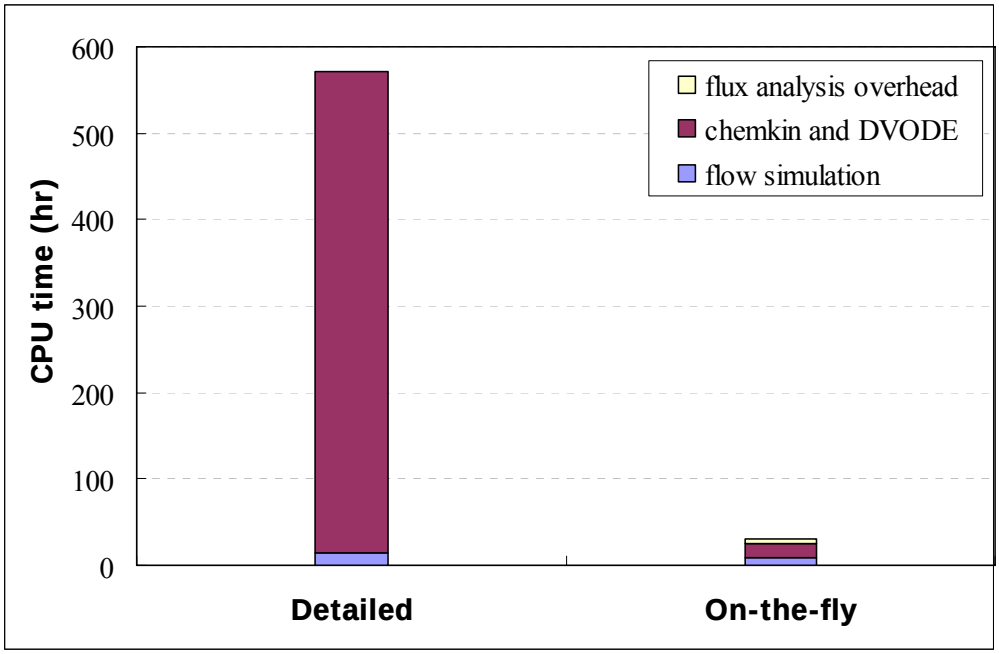

Figure 3.6: CPU time distribution of detailed simulation and on-the-fly scheme of n-pentane combustion in KIVA.

3.2 Characterization of advanced combustion process with detailed chemistry

3.2.1 CFD model and numerical cases

The on-the-fly mechanism reduction framework enables integration of detailed chemistry in CFD calculations. By fully integrating detailed chemistry and realistic flow simulation, an accurate prediction of in-cylinder combustion behavior as well as combustion parameters, such as pressure, temperature, and species compositions, can be obtained for HCCI engines. Thus the on-the-fly reduction frame work provides a useful tool to numerically investigate complex combustion processes by taking advantage of detailed chemistry. The information provided in such simulations is not available when using simplified chemistry model in reactive flow simulations. Taking HCCI engines for example, HCCI has received increasing attention from the engine community as a promising alternative operation mode to conventional Diesel and Spark-Ignited (SI) engines. Its potential to achieve Diesel-like combustion efficiency and reduce NOx and soot emissions have been reported (Dec 2009; Dibble 2001; Flowers 2000). However, the main obstacle in the application of HCCI is the lack of reliable ignition timing controlling strategies (Dec 2009). The control issue stems from multiple ignition sites in the chamber and cycle-to-cycle variations (Dec 2009; Dibble 2001; Oevermann, Schmidt et al. 2008). Various controlling strategies, including Direct Injection (DI) (Marriot 2001), Variable Valve Actuation (VVA) (Law 2001), and Exhaust Gas Recirculation (Choi, Han et al. 2004; Kim and Lee 2006; Lu, Chen et al. 2005), have been investigated to achieve accurate ignition timing control. Accurate simulation of these processes requires realistic flow simulation as well as detailed chemistry.

The main focus of this section is to implement the on-the-fly reduction approach in CFD code to, for the first time, integrate highly complex fuel mechanisms in every computational cell and time step. By fully integrating detailed chemistry and realistic flow simulation, an accurate prediction of in-cylinder combustion behavior as well as combustion parameters, such as pressure, temperature, and species compositions, can be obtained for HCCI engines.

Engine CFD code KIVA-3V is employed is this study to simulate HCCI engine combustion. The fuel is n-heptane and a detailed n-heptane oxidation mechanism including 653 species and 2827 reactions (Curran, Gaffuri et al. 1998; Mehl 2009a; Mehl 2009b) is used to simulate diesel combustion in HCCI engines. A 99.9% cutoff is in the on-the-fly reduction to retain high fidelity to the detailed mechanism. The numerical mesh used for the analysis is the same grid as shown in Figure 3.1. The validation case we examined is to simulate the direct injection mode using room temperature, atmospheric-pressure spray in HCCI engines. The initial conditions of the numerical model is prescribed by the in-cylinder fuel concentration distribution obtained in laser-induced exciplex-fluorescence (LIEF) experiments (Fansler, Drake et al. 2009). When the fuel is injected into the chamber at room temperature, fuel vaporization is slow and thus a large portion of the fuel hit the piston in liquid state. This portion of fuel vaporizes as the piston brings it up to the cylinder head during compression. Meanwhile, there are fuel droplets remaining on the injector, resulting in moderately higher fuel concentration near the injector. A numerical case simulating the fuel concentration inhomogeneity induced by fuel spray in this scheme is investigated in this study. The initial fuel concentration distribution in the cylinder is shown in Figure 3.7. The

simulation starts from crank angle (CA) -80.0° After Top Dead Center (ATDC). The fuel concentration is stratified with global equivalence ratio 0.32, and the temperature is uniformly 498K in the chamber at -80.0° ATDC. The equivalence ratio ranges from 0.1 to 1.6, covering the span of fuel concentration encountered in HCCI engines operated in direct injection mode. This case is designed to study the in-cylinder combustion behavior under inhomogeneous fuel concentration. The stratified HCCI combustion also provides an ideal test case to validate the adaptability of the proposed on-the-fly reduction method in addressing different reactive conditions. The inhomogeneous case is compared to a homogeneous case with the same initial charge as the global average of the inhomogeneous case, equivalence ratio 0.32 and temperature 498 K, at -80.0° ATDC.

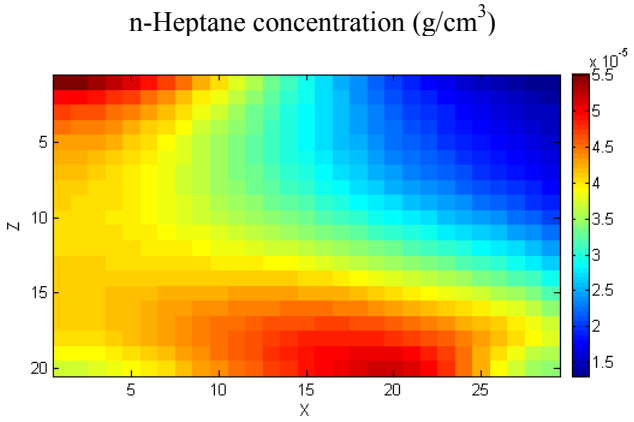

Figure 3.7: Initial n-heptane concentration distribution in the engine chamber of the stratified case.

3.2.2 Effects of charge stratification on temperature and pressure in HCCI engines

When homogeneous charge is used in HCCI engines, the engine chamber ignite simultaneously, which results in a high pressure-rise rate (PRR) and short combustion duration. Too high PRR might cause engine knock, thus sometimes it is necessary to introduce inhomogeneities to lower PRR and extend combustion duration (Dec 2009;

Dibble 2001; Kim and Lee 2006; Lu, Chen et al. 2005). The average in-cylinder temperature, heat release rate (HRR), and pressure of the two cases are shown in Figures 3.8 and 3.9. Both stratified and homogeneous cases exhibit pronounced cool flame behavior (-45° ATDC to -43° ATDC). Significant amount of heat is released in the cool flame stage and temperature was increased by 50-100 K. The main ignition occurs earlier in the stratified case due to the fact that fuel rich region releases more heat than the homogeneous chamber in the pre-ignition stage (CA -35° to -33°). The stratified charge also extends the duration of heat release by nearly 2 crank angles. This is due to non-instantaneous ignition in the stratified case, which will be illustrated in the following sections. As indicated by arrows in Figure 3.8, significant amount of heat is released after the main ignition in the stratified case, which results in longer heat release duration and lower peak HRR in the stratified case.

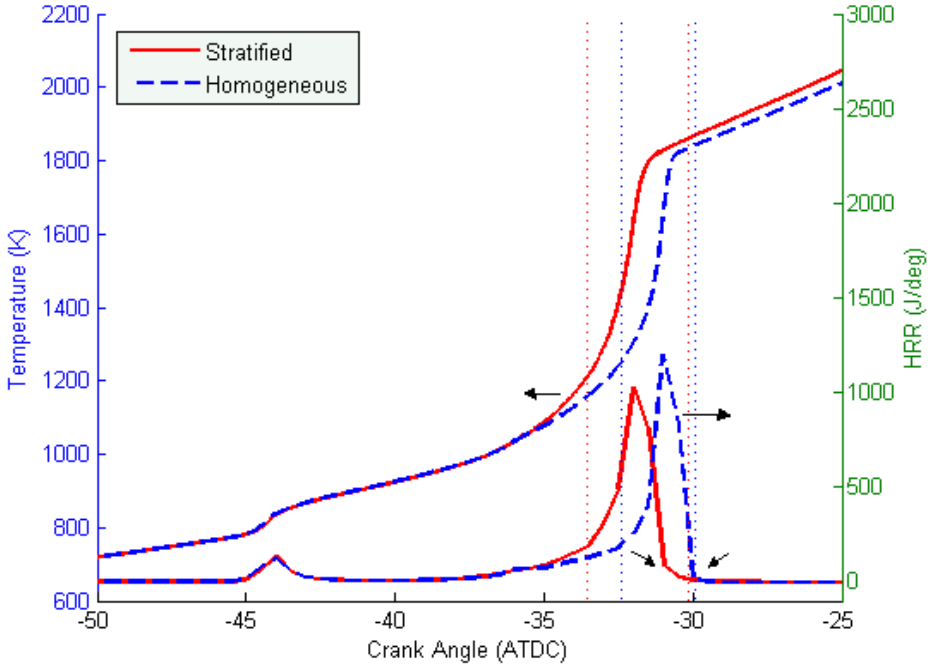

Figure 3.8: Temperature and heat releasing rate (HRR) profiles of the stratified case (solid lines) and the homogeneous case (dashed lines).

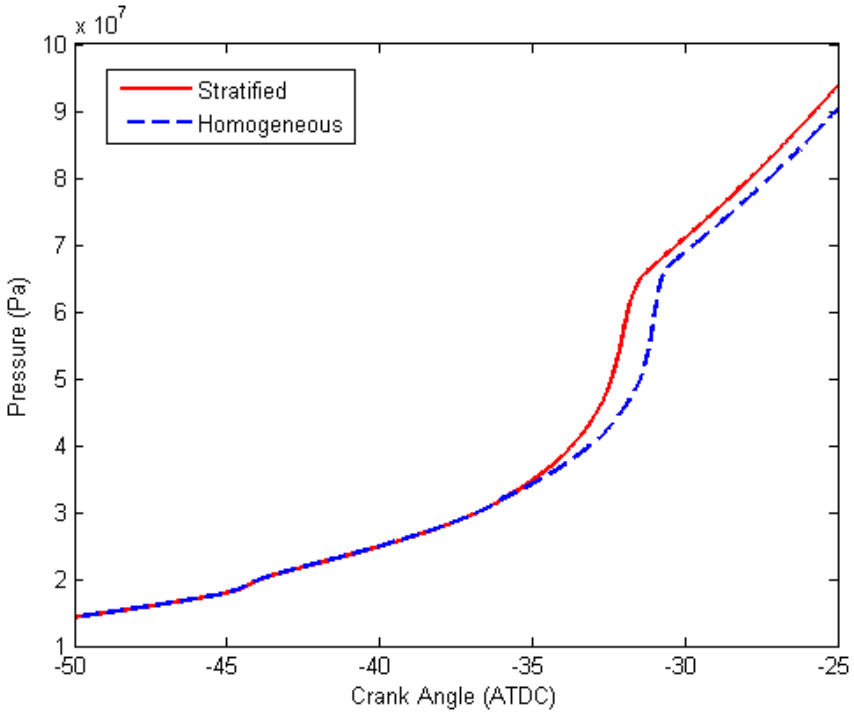

Figure 3.9: Pressure profile of the stratified case (solid lines) and the homogeneous case (dashed lines).

3.2.3 Effects of charge stratification on in-cylinder combustion process

To analyze the underlying mechanism of the effects of stratification on HCCI combustion, it is necessary to capture in-cylinder temperature and species composition distributions at different crank angles. By solving the detailed chemistry for each computational cell, the on-the-fly reduction model tracks compositions of all species and thus enables a detailed characterization of the in-cylinder combustion behavior. In-cylinder temperature, fuel concentration, and oxygen concentration distributions at different crank angles are shown in Figures 3.10 and 3.11. In the stratified case, the fuel vaporization results in a stratification of equivalence ratio in the chamber, with high fuel concentration near the cylinder center and low fuel concentration near the wall. At the early stage of the compression, endothermic n-heptane decomposition represents the main chemical activity, which results in lower temperature in fuel rich regions. When the cylinder is further compressed, in-cylinder temperature elevates and fuel rich regions exhibit low temperature flame behavior. The heat released from the low temperature oxidation reactions elevates the temperature of fuel rich regions to a higher level than fuel lean regions. The chamber finally ignites in the region between fuel rich and fuel lean regions. In the homogeneous case, as shown in Figure 3.11, multiple ignition sites are developed simultaneously around CA -32.7° ATDC. These ignition sites cover a large portion of the chamber, generating a near-instantaneous thermal explosion. This thermal explosion results in a high pressure-rise rate and heat release rate, which might cause engine knock (Dec 2009; Oevermann, Schmidt et al. 2008). On the contrary, the subsonic flame propagation in the inhomogeneous case extends the burn duration and gives rise to a less steep pressure-rise.

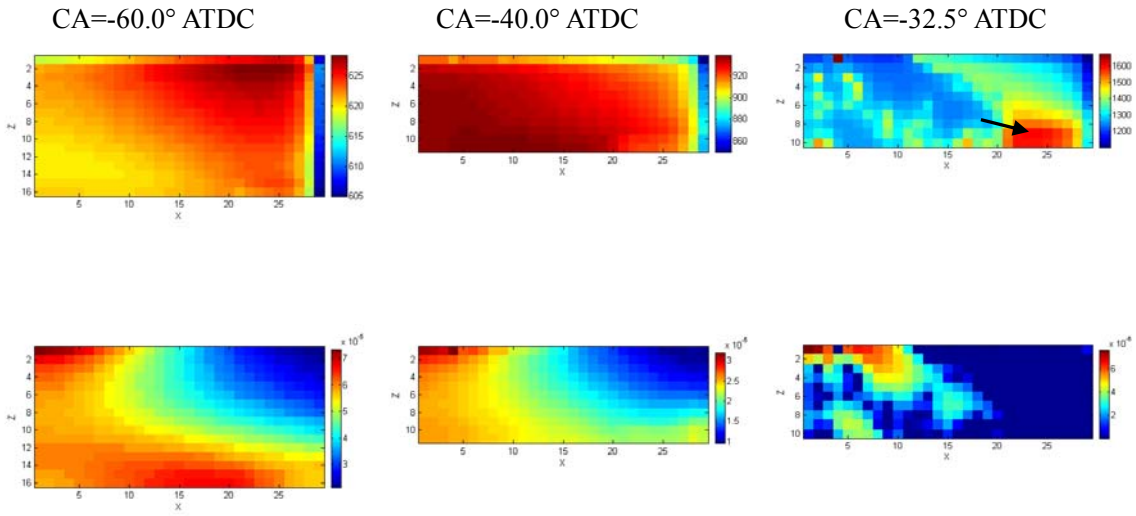

Figure 3.10: In-cylinder temperature and n-heptane concentration distributions at different crank angles of the stratified case. Top row: temperature (K); bottom row: n-heptane concentration (g/cm^3).

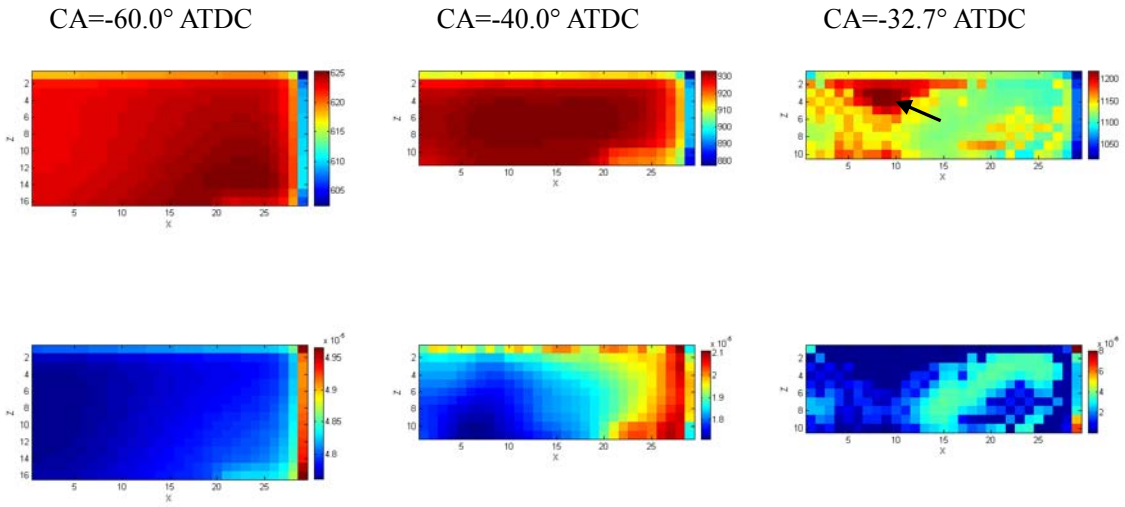

Figure 3.11: In-cylinder temperature and n-heptane concentration distributions at different crank angles of the homogeneous case.

3.3 Summary

An on-the-fly reduction scheme is implemented to integrate detailed chemistry and CFD simulations. A detailed n-heptane mechanism including 653 species and 2827 reactions is used in the simulation of HCCI engine combustion. By using the proposed on-the-fly reduction method, detailed chemistry is solved for each computational cell and each time step of the CFD simulation. A stratified HCCI combustion case was investigated numerically and compared to a homogeneous HCCI case. In-cylinder combustion behaviors as well as combustion parameters, such as pressure, temperature, and species compositions in HCCI combustion are captured. Multiple ignition sites are predicted in the homogeneous case while only one ignition site is observed in the stratified case. Flux analysis is employed to investigate the underlying chemical reaction scheme of different regions. It was found that high temperature oxidation pathways of n-heptane are the most active in both stratified and homogeneous HCCI combustion. However, the high temperature pathways are less dominant in the stratified combustion, with one third flux transitions going through low temperature and medium temperature pathways. By solving the detailed chemistry for each computational cell and time step, the on-the-fly reduction model provides a detailed characterization of in-cylinder combustion behaviors of HCCI engines, which is essential to predict multiple ignition sites and distinct chemical kinetics at different regions during the combustion process. The on-the-fly framework provides an efficient yet accurate mechanism reduction approach to take advantage of detailed chemistry in the investigation of complex reactive flows.

Chapter 4

Extending the On-the-fly Reduction Approach to Multi-network Reaction Systems

In the previous chapter, we have introduced and demonstrated an on-the-fly kinetic reduction method based on element flux analysis. Element flux analysis provides an indicator to quantify species activity, which can be implemented in mechanism reduction to identify redundant species and reactions. Since the combustion process described in the previous chapter mainly involves hydrocarbon oxidation, only carbon element flux was incorporated in order to capture carbon transformations. However, when the flux analysis is to be extended to systems that involve NOx formation, it becomes necessary to incorporate multi-element analysis in the reduction scheme in order to capture different reaction networks in the system. Another drawback of the proposed reduction scheme is that soot formation can not be well captured during the reduction procedure. This is due to the fact that soot species usually have much smaller flux comparing to fuel oxidation network. Therefore when the element flux pointers are sorted to identify key species, soot species are always below the cutoff and excluded from the reduced mechanisms. Moreover, although nitrogen flux can uniquely capture NOx formation network, there is no unique element for soot formation network.

To address the aforementioned limitations of the reduction scheme, an efficient multi-element (C, H, O, N) flux analysis framework combined with a graph searching

procedure are introduced in this work to incorporate NOx formation and soot formation in the reduced mechanisms. The proposed method is demonstrated using a JP-10 mechanism (Li, Varatharajan et al. 2001) with NOx and soot formation (Richter 2005). JP-10 is a single-component hydrocarbon ($C_{10}H_{16}$) aviation turbine fuel which is used in volume-limited combustion chambers such as those of supersonic-combustion ramjets and pulse-detonation engines. The high energy density, as well as the very low freezing point of the fluid has made JP-10 the only air-breathing missile fuel used by the United States at the present time (Bruno 2006). Unlike other practical fuels, JP-10, being a pure component, is amenable to theoretically modeling. The JP-10 decomposition and combustion mechanism used in this work was proposed by Li et al. (Li, Varatharajan et al. 2001) which employed a number of approximations in the decomposition of JP-10 to species of smaller size. Despite its brevity in JP-10 decomposition, the mechanism is capable to accurately predict the ignition delay times (Li, Varatharajan et al. 2001; Nakra, Green et al. 2006) and the combustion of smaller molecules formed in JP-10 decomposition (Nakra, Green et al. 2006; Petrova and Williams 2006).

4.1 Multi-element flux analysis to capture NOx formation

For a complete characterization of the combustion process, multiple element flux analysis involving C, H, O, and N transformations should be taken into account, rather than only considering carbon flux for hydrocarbon oxidation systems. Once calculated and sorted respectively, a user-selected cutoff is applied to the corresponding flux lists. Species above the cutoff correspond to larger flux and are retained in the reduced mechanism. Meanwhile, species below the cutoff are of trivial activity, and are excluded from current reduced mechanism. Note here fluxes for each element are calculated and cut separately.

The union set of reduced species sets for each element defines the reduced mechanism. This is due to the fact that different elements might have different flux values. If all element fluxes are sorted together, C, H, and O element fluxes will be much larger than N flux. Thus species with C, H, and O fluxes will be given higher rank while N-bearing species are always excluded from the reduced mechanism. To account for this variance, fluxes based on different elements are sorted and considered separately. While the element flux indicators provided by flux analysis describe the transition between two species, they also illustrate important connections between fuels and final products. These flux indicators can be used to identify the key pathways present in a detailed kinetic mechanism with minimum computational effort. By monitoring flux pointers in a dynamic mode, different stages of the system evolution can be captured.

To better illustrate the flux analysis methodology, we consider the stoichiometric JP-10/air oxidation and NOx formation in a plug flow reactor (PFR) model with initial temperature 800 K. First, flux analysis is performed for elements C, O, H, and N of JP-10 combustion in PFR to show the transition of different elements in the system. Element flux pointers at different stages are listed in Table 4.1. Due to the limitation of space, only the first 10 source-sink pairs out of hundreds of pairs are shown. At the initial stage of combustion (T=805K), JP-10 decomposition is the dominant part of the entire pathway. As shown in Table 4.1, carbon flux analysis captures active hydrocarbon species at initial stage, most of which are from JP-10 decomposition reactions (Reactions 1 - 3).

$$C_{10}H_{16} \rightarrow C_2H_2 + 2C_2H_4 + C_4H_6 \qquad \text{Reaction 1}$$

$$C_{10}H_{16} \rightarrow H + C_2H_4 + C_3H_3 + C_5H_8 \qquad \text{Reaction 2}$$

$$C_{10}H_{16} \rightarrow H + C_2H_2 + C_3H_5 + C_5H_8 \qquad \text{Reaction 3}$$

It should be pointed out that these reactions are not elementary reactions. Instead, some overall approximations were employed to combine series of elementary reactions steps. This is due to the fact that JP-10 is too large a molecule for a complete detailed chemical mechanism of its decomposition and combustion to be developed, which was indicated by the mechanism authors (Li, Varatharajan et al. 2001). Hydrogen flux captures active H-bearing radicals and species such as H, HO_2 as well as hydrocarbon species. Oxygen flux identifies active O-bearing radicals and species such as O_2, OH, and O. Most of these active species captured by hydrogen and oxygen flux are involved in facilitated JP-10 decomposition. Active species of NOx formation can be identified though the associated N fluxes, although flux values are much smaller than carbon, hydrogen, and oxygen. As the system temperature increases to 1500 K, oxidation of small hydrocarbons such as C_2H_2 and C_2H_4 become dominant. For the NOx formation network, similar source-sink pairs have been identified with flux magnitudes increased by a factor of 10. When the system temperature further increases to 2700 K, the combustion process reaches the final stage, where reactions from intermediates to final products CO_2 and H_2O become dominant. Meanwhile, high temperature significantly promotes NOx formation: flux values are increased by a factor of 100 compared to the initial stage. NO, NO_2, and N_2O are formed with highest rates throughout the combustion process. As shown in Table 4.1, a small portion of source-sink pairs can capture most of the element transformation in the system. This is due to the fact that at certain phase of a combustion process, only part of the overall pathway is active while the rest shows little or no activity. Thus, as the combustion process evolves different components of the pathway become active.

Table 4.1: Element flux of stoichiometric JP-10/air combustion with NOx formation. Initial temperature T=800 K.

	C			O			H			N		
T=805K	JP-10	C5H8	1401.3	O2	HO2	1057.1	JP-10	C5H8	2150.4	N2	N2O	0.0159
	C3H5	C3H6	655.6	OH	H2O	294.2	C3H5	C3H6	1078.6	N2	N	0.0001
	JP-10	C3H5	514.3	O2	O	214.9	JP-10	C3H5	821.6	N2	HCN	0.0001
	C5H8	C3H4	423.3	CH2CHO	CH2CO	187.0	C5H8	C3H5	688.3	N	NO	0.0001
	C5H8	C3H5	423.3	HO2	H2O2	181.6	C5H8	C3H4	550.7	N2	N2H	0.0000
	JP-10	C2H4	373.9	O2	CH2CHO	179.0	C2H3	CH2CHO	537.1	NO	NO2	0.0000
	JP-10	C2H2	364.2	HO2	OH	167.5	JP-10	C2H4	503.4	N2H	N2O	0.0000
	C2H3	CH2CHO	358.1	O2	CO	138.4	C5H8	C2H3	413.0	N2O	NO	0.0000
	JP-10	C3H3	326.5	O2	OH	120.1	JP-10	H	250.2	N2O	NH	0.0000
	C5H8	C2H2	284.3	O	OH	96.6	C5H8	HO2	221.0	NO	HNCO	0.0000
T=1500K	HCO	CO	897.6	O2	OH	1049.6	H	OH	1366.8	N2	N2O	0.1743
	CH2O	HCO	746.9	O2	HO2	927.0	CH2CO	CH3	1053.6	N2	N	0.0450
	C2H4	C2H3	722.3	O2	O	871.1	H	CH3	934.7	N2	HCN	0.0449
	CH2CO	CO	704.0	OH	H2O	864.1	C2H4	C2H3	868.1	N	NO	0.0369
	C2H2	HCCO	622.7	O2	CO	699.4	OH	H2O	822.8	N2	N2H	0.0040
	CH2CHO	CH2CO	570.8	HCO	CO	566.4	H	H2	768.6	NO2	NO	0.0037
	HCCO	CO	548.8	CH2CO	CO	498.8	C2H3	CH2CHO	716.9	N2O	NO	0.0028
	CH2CO	CH3	526.8	CH2O	HCO	475.6	HCO	H	660.6	N2O	NH	0.0025
	C2H2	CH2CO	521.9	HO2	OH	459.4	CH3	CH2O	601.3	NO	HNCO	0.0012
	C2H3	CH2CHO	477.9	O2	CO2	279.1	CH2CHO	CH2CO	570.8	NH	HNO	0.0012
T=2200K	CO	CO2	21.3	OH	H2O	27.0	OH	H	47.3	N2	NO	2.2828
	CO	HCO	0.2	CO	CO2	21.2	OH	H2O	36.8	N2	N	2.2696
	HCO	CO2	0.0	OH	CO2	20.9	OH	HO2	16.7	N	NO	2.2317
	CO	NCO	0.0	OH	HO2	20.4	H	H2O	15.7	N2	N2H	0.2782
	C2H4O	CO	0.0	O2	OH	19.5	H2	H	9.0	HNO	NO	0.2519
	C2H4O	CH3	0.0	O2	O	18.4	HO2	H2O	5.6	NO	NO2	0.0870
	CH2O	HCO	0.0	O	OH	15.4	H2	OH	4.5	NH	NO	0.0568
	CH3	CH2O	0.0	HO2	O2	12.7	H2	H2O	4.3	N2H	N2O	0.0564
	C2H4O	C2H4	0.0	O	HO2	12.1	H	HO2	1.8	N2O	NO	0.0420
	CH3	S-CH2	0.0	HO2	H2O	4.2	HO2	H2	0.9	N	NH	0.0357

4.2 Graph searching to identify soot formation network

The proposed reduction scheme is able to capture the reactive propensity of systems with NOx formation by employing multi-element flux analysis. However, when the scheme is applied to hydrocarbon oxidation mechanisms with soot formation, soot species and precursors, also analyzed through C-fluxes, are usually given low ranks due to their small flux values compared to fuel oxidation network. It should be pointed out that in our illustration using JP-10/NOx, although the NOx formation network also has much smaller flux compared to JP-10 oxidation, the reactive propensity of N-bearing species can be captured by nitrogen element flux. However, a soot formation network usually consists of polycyclic aromatic hydrocarbons (PAH) evolution and their aggregation to soot, which involves the same elements (C, H, and O) as fuel oxidation. Thus there is no unique element that can capture soot formation separately. In order to incorporate soot formation kinetics in mechanism reduction, a kinetic network separation algorithm should be incorporated in the on-the-fly scheme. The objective of this procedure is to separate the soot formation network from the fuel oxidation network. The species in the two separate networks are analyzed and reduced independently based on element flux. Then the two reduced species sets are combined and reactions only involving species in the combined set are kept in the reduced mechanisms. Identifying the reaction set based on the combined species set ensures that interactions between different networks will be included in the reduced mechanism.

For the separation of two kinetic networks explore concepts similar to graph partitioning, i.e, the process of dividing a graph into pieces, algorithms. There are three major categories of graph partitioning algorithms: (a) spectral methods (Karypis and Kumar

1998b; Karypis and Kumar 1998a), which seek a partition that maximize the intra-community connections while minimizing inter-community connections based on adjacency matrix; (b) recursive partitioning (Hsieh, Paulino et al. 1995), which start the partitioning procedure by dividing the original graph into a certain number of sub-graphs and further divide them if desired; and (c) local agglomeration (Prasad and Skourikhine 2005; Prasad and Skourikhine 2006), in which sub-graphs are agglomerated, based on selected nodes, until certain criteria are satisfied. The sub-graphs identified by spectral methods have the maximum intra-community connectivity; however, the sub-graphs might include both soot species and fuel oxidation species. Therefore, the method is unable to effectively separate the soot formation from the fuel oxidation network. Recursive partitioning methods can provide a partition of the original graph with user-defined number of sub-graphs. However, when implemented in our work to separate different reaction networks, recursive partitioning also fails to discriminate soot formation species and fuel oxidation species. Local agglomeration method starts from specific nodes and groups neighboring nodes based on the strength of connections. It is able to separate different sub-networks by initializing agglomeration from species that are exclusively involved in each sub-network, which well serves the purpose of network separation in this work. In the present study, since both the soot formation and fuel oxidation originate from JP-10, we employ reverse agglomeration which starts from the final products of the two sub-networks. PAHs and CO_2 are selected to initialize the soot formation and fuel oxidation agglomeration respectively. The algorithm takes PAHs and CO_2 as tree root and searches backward the entire reaction network to identify their source species. Then these source species are considered as sink species in next iteration.

The algorithm proceeds until no new sources can be identified. After completion of the searching part, soot formation and JP-10 oxidation sub-networks that terminate at PAHs and CO_2, respectively, are separated. Figure 4.1 shows the soot formation (red edges) and JP-10 oxidation (black edges) sub-networks. For simplicity, only a part of the graph is shown. It can be observed from the flux graph that overlap exists between the two sub-networks (blue edges). The overlapping part is assigned to the fuel oxidation network because source-sink pairs in this part have comparable flux magnitudes to the fuel oxidation network, while being much greater than the corresponding components of the soot formation network. For the JP-10/soot mechanism used in the present work, the entire flux graph constitutes of 748 edges, 58 of which are located in the soot formation network and 690 are included in JP-10 oxidation network. Given the two separate sub-networks, flux analysis is employed on each sub-network to identify active soot formation and reduced JP-10 oxidation species. Two reduced species sets are then combined and reactions involving these active species are identified to form the kinetic mechanism for given time step.

The mechanism reduction scheme based on flux analysis provides an efficient method to couple detailed chemistry with CFD calculation. The on-the-fly reduction scheme, as the name suggests, involves the dynamic identification of reduced mechanisms during the simulation. In practice, element flux analysis is carried out at every time step of the CFD calculation and a reduced mechanism is developed based on the active species and reactions identified from flux analysis. The reduced mechanism defines the chemistry of the current time step and species in the reduced mechanism are integrated. However, all the species are transported and all species concentrations are stored in the flow

calculation so that when a different set of active species are identified at other time steps, the required species information can be retrieved to initialize the kinetic calculation for the given time step.

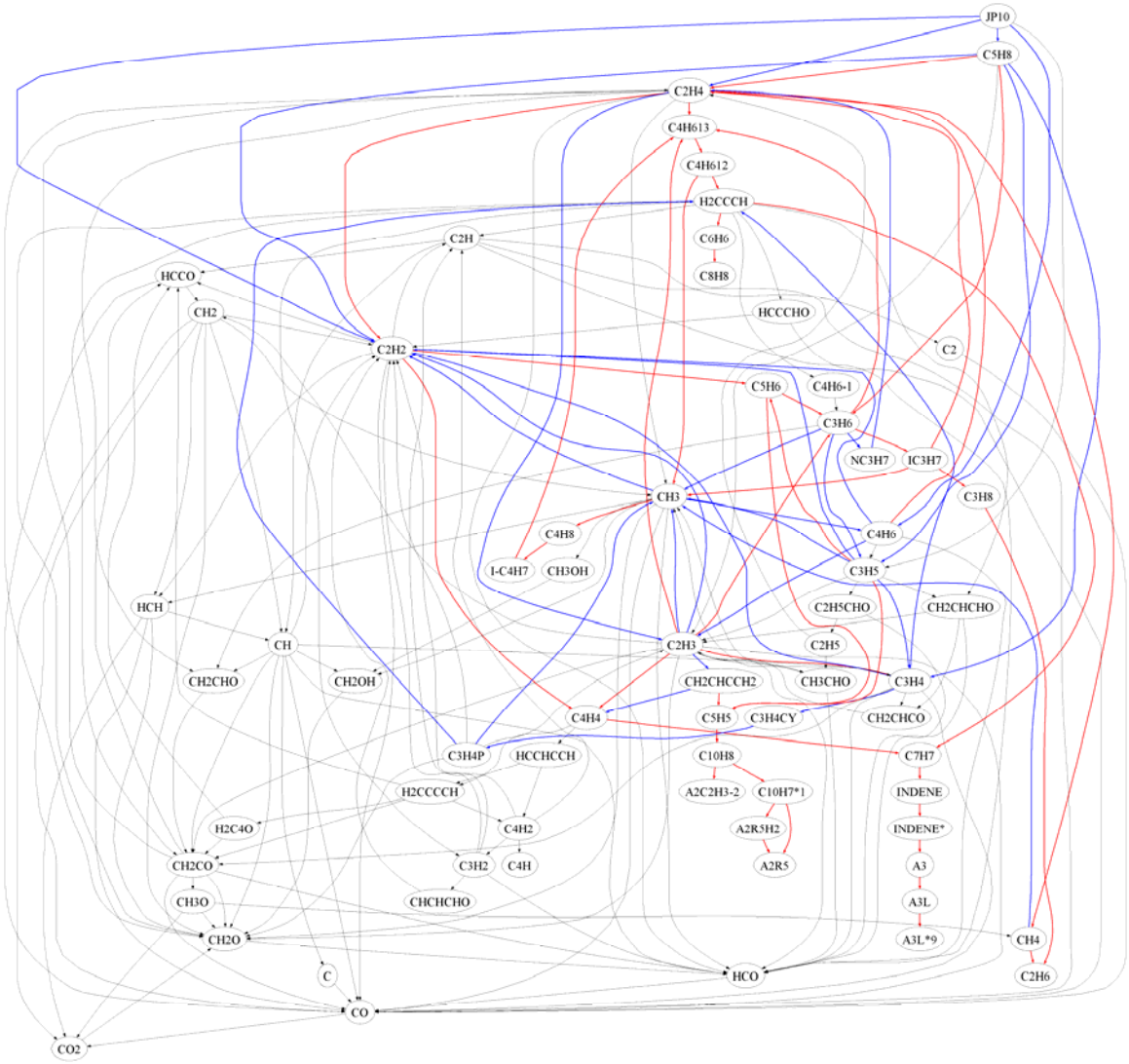

Figure 4.1: Flux graph of JP-10 oxidation with PAH formation. Red edges: PAH formation network; black edges: JP-10 oxidation network; blue edges: overlap of two networks.

4.3 Characterization of NOx and soot formation in combustion processes

The proposed element flux analysis is demonstrated using a JP-10/NOx chemical mechanism consisting of 56 species and 260 reactions (Li, Varatharajan et al. 2001). Predicted results with the on-the-fly reduction method are compared with simulations with the detailed mechanism and the experimental data of Mikolaitis et al. (Mikolaitis, Segal et al. 2003) in Figure 4.2. The on-the-fly reduced representation reproduces the ignition delay of JP-10 with good agreement compared to detailed simulations.

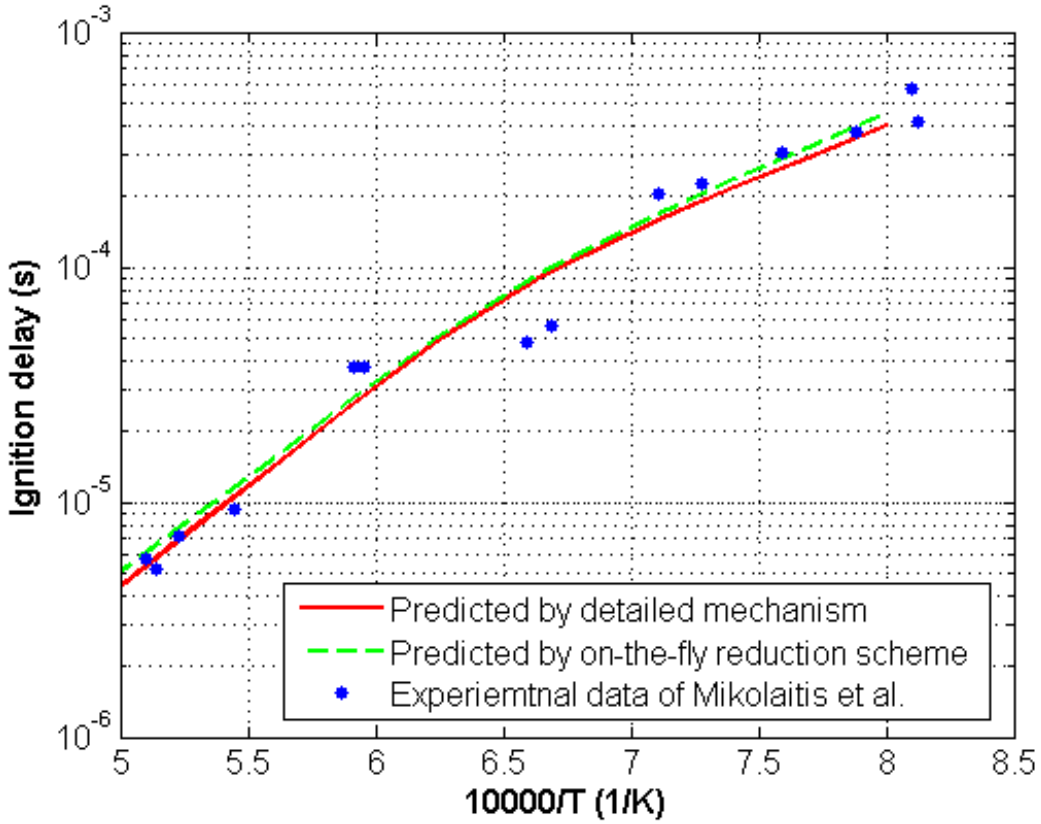

Figure 4.2: Ignition delay time of stoichiometric JP-10/air combustion predicted by simulations using detailed mechanism and on-the-fly reduction scheme compared with experimental data.

The proposed on-the-fly scheme based on multi-element flux analysis is integrated with the KIVA-3V CFD code (Amsden 1997) to predict JP-10 combustion and NOx formation. The 2-dimensional numerical mesh introduced in the previous Chapter is employed to simulate homogeneous charge compression ignition (HCCI) engine. CHEMKIN (Kee 1996) is used for solving the chemistry during the engine simulation. The model simulates combustion in a HCCI engine from crank angle -40° to 40° ATDC. Temperature and pressure profiles predicted by the detailed simulation and the on-the-fly reduction scheme are illustrated in Figure 4.3. Both the ignition timing and the peak temperature and pressure can be reproduced by the on-the-fly scheme with good agreement. Selected species profiles of JP-10 oxidation and NOx formation are compared in Figure 4.4.

The reduced mechanism sizes for JP-10 oxidation and NOx formation are compared in Figure 4.5 in terms of species numbers. At the initial stages, the decomposition of JP-10 is the most significant part of the reaction network, thus small mechanisms were generated including only JP-10 and its decomposition products. During the induction stage, the mechanism size of JP-10 network grows due to the increased activity of JP-10 decomposition and radical pool build-up. When the system ignites, large amount of radicals and intermediate species are generated which results in even larger JP-10 oxidation network. The size of JP-10 oxidation reaches its maximum level at the beginning of the ignition stage, at which point molecules and radicals have the highest activity. However, it can be observed in Figure 4.5 that the NOx formation network evolves through a different pattern. The network grows after the system ignites. This is due to the fact that the oxidation of N_2 may occur only when the system temperature

reaches certain level. After ignition, high system temperature expedites N_2 dissociation, which initiates NOx formation. The network size evolution shown in Figure 4.5 indicates that NOx formation lags fuel oxidation in the combustion process.

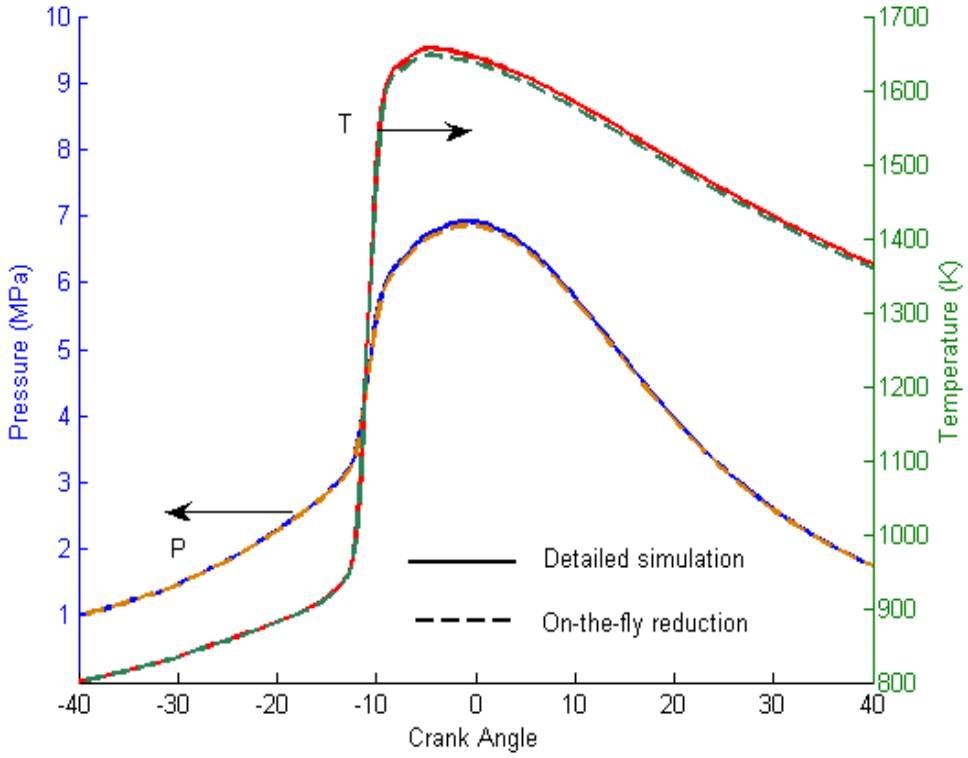

Figure 4.3: Temperature and Pressure profiles of stoichiometric JP-10/air oxidation with NOx formation in KIVA simulation. Initial conditions: T=800 K, P=1 MPa.

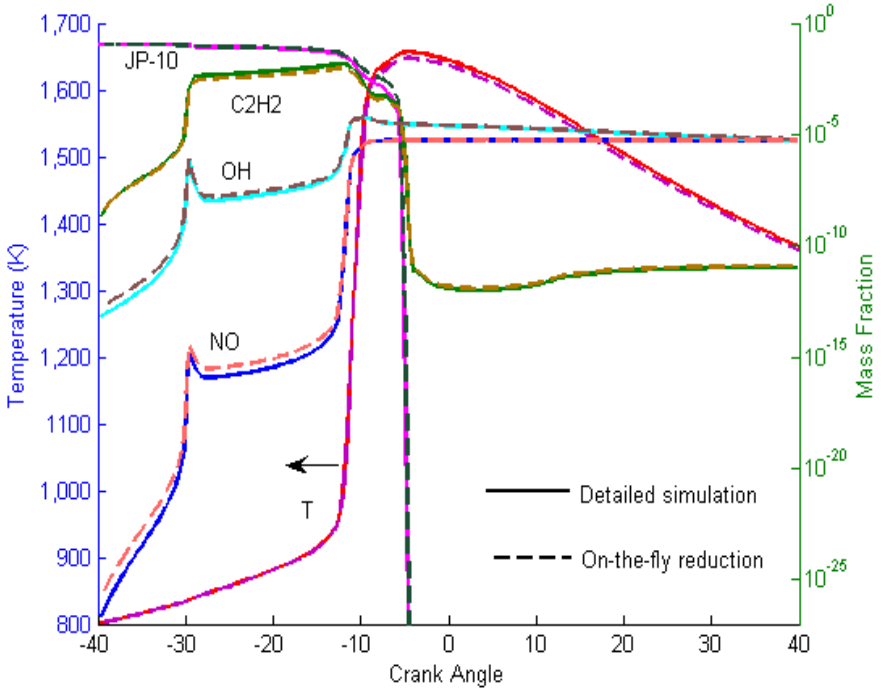

Figure 4.4: Selected species concentration profiles of stoichiometric JP-10/air oxidation with NOx formation in KIVA simulation. Initial conditions: T=800 K, P=1 MPa.

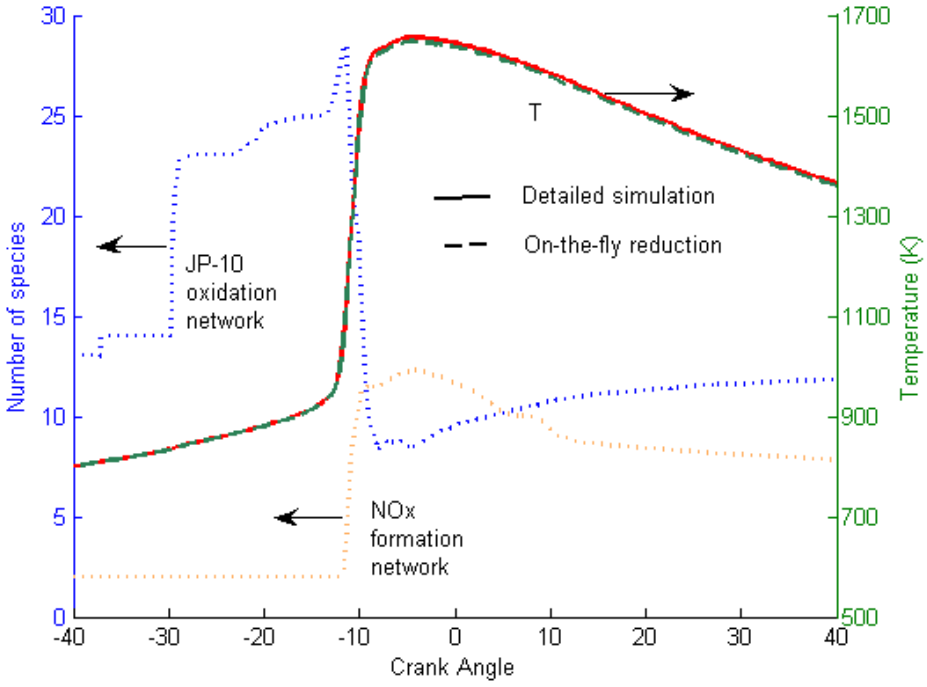

Figure 4.5: Mechanism size of stoichiometric JP-10/air oxidation with NOx formation. Initial conditions: T=800 K, P=1 MPa.

In order to capture soot formation in JP-10 combustion, the proposed graph searching technique and the on-the-fly reduction scheme is applied on a JP-10/soot mechanism constitute of 161 species and 900 reactions which is created by combining a JP-10 mechanism and a PAH formation mechanism. The JP-10 decomposition and oxidation kinetics is from the JP-10 oxidation mechanism (Li, Varatharajan et al. 2001) and the kinetics of C2-C5 oxidation and PAH formation are described by the mechanism developed by Richter et al. (Richter, Benish et al. 2000). The tree-building search algorithm described in the previous section is employed to separate soot formation sub-network from the fuel oxidation network. The KIVA simulation is monitored from crank angle -40° to 40° ATDC for stoichiometric JP-10/O_2/Ar combustion with an initial temperature of 800 K and pressure 1 MPa.

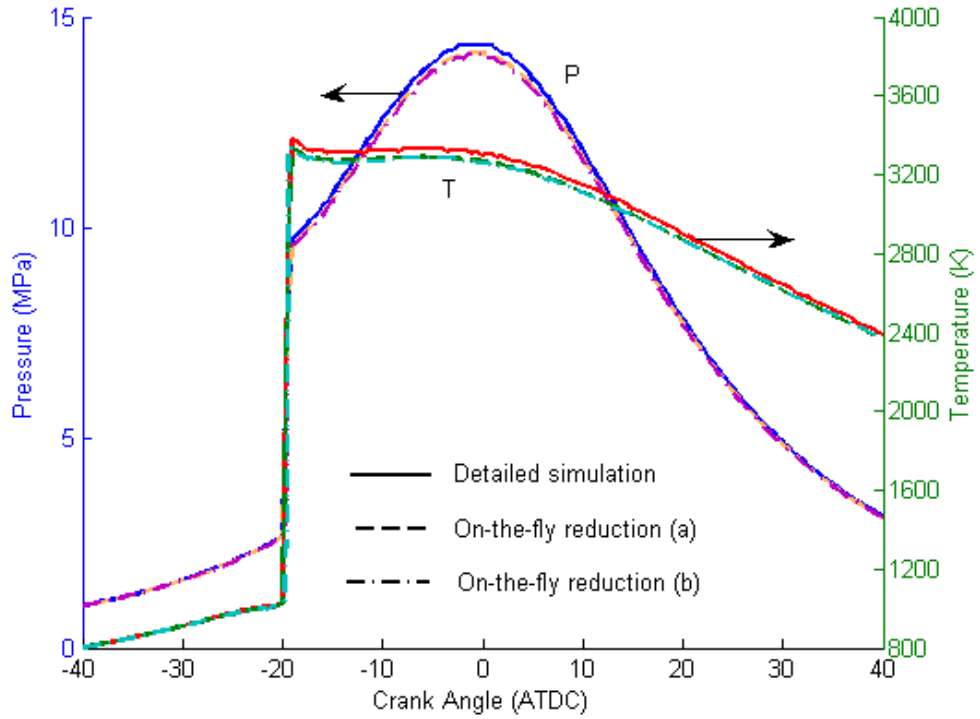

Figure 4.6: Temperature and Pressure profiles of stoichiometric JP-10/air oxidation with soot formation in KIVA simulation. (a) soot formation separated from JP-10 oxidation, (b) soot formation not separated from JP-10 oxidation. Initial conditions: T=800 K, P=1 MPa.

Figure 4.6 compares temperature and pressure profiles of the detailed simulation, the on-the-fly reduction on two separate flux graphs (scheme a), and the on-the-fly scheme without separation of soot formation from JP-10 oxidation (scheme b). It can be observed in Figure 4.6 that applying different analysis schemes for the soot network does not affect significantly the temperature and pressure profiles. This is due to the fact that soot formation has very small flux and thus makes only a very small contribution to thermo-physical properties of the system such as temperature and pressure. However, the affect of properly accounting for soot formation are significant where considering the overall combustion process. Figure 4.7 compares the profiles of JP-10, C_2H_2, and $C_{10}H_8$ concentration of scheme a and scheme b. $C_{10}H_8$ is one of the major PAHs formed in hydrocarbon combustion and C_2H_2 plays an important role in PAH formation (Richter 2005). Thus these two species are characteristic of soot formation network and are chosen in order to compare different analysis schemes in this work. It can be seen in Figure 4.7 that JP-10 concentrations are not affected too much by two different schemes since soot formation consumes very small portion of hydrocarbons in the system. On the other hand, C_2H_2 and $C_{10}H_8$ exhibit distinct profiles in the two different schemes. In scheme (a), where soot network is separated from JP-10 oxidation, C_2H_2 and $C_{10}H_8$ are predicted accurately compared to the detailed simulation, while in scheme (b), where reduction is done on the entire network, soot formation network are not included in the reduced mechanisms due to their small flux. Therefore the mass fraction of C_2H_2 after ignition is much higher in scheme (b) since soot formation is not included and C_2H_2 is less consumed. Similarly, in scheme (b) $C_{10}H_8$ is not well predicted because only after the ignition when the flux of JP-10 oxidation network drops to a low level, soot formation

network can have higher rank and are considered in the reduced mechanisms. Thus before ignition no $C_{10}H_8$ is produced, and after ignition $C_{10}H_8$ starts to accumulate, but is still much lower than the detailed simulation results.

4.4 Summary

A multi-element flux analysis has been proposed to address transitions and transformations of different elements in the system. Element flux of carbon, oxygen, and hydrogen are analyzed separately to capture fuel oxidation and radicals transition. In addition, nitrogen flux is used to describe NOx formation in the system. However, for soot formation there is no unique element that can capture the network. In order to include soot formation in kinetic reduction, a network separation algorithm has been complemented to the on-the-fly reduction scheme. Soot formation network and fuel oxidation network are identified by searching from PAHs and CO_2, respectively. The two networks are reduced separately and two reduced mechanisms are combined to define local chemistry.

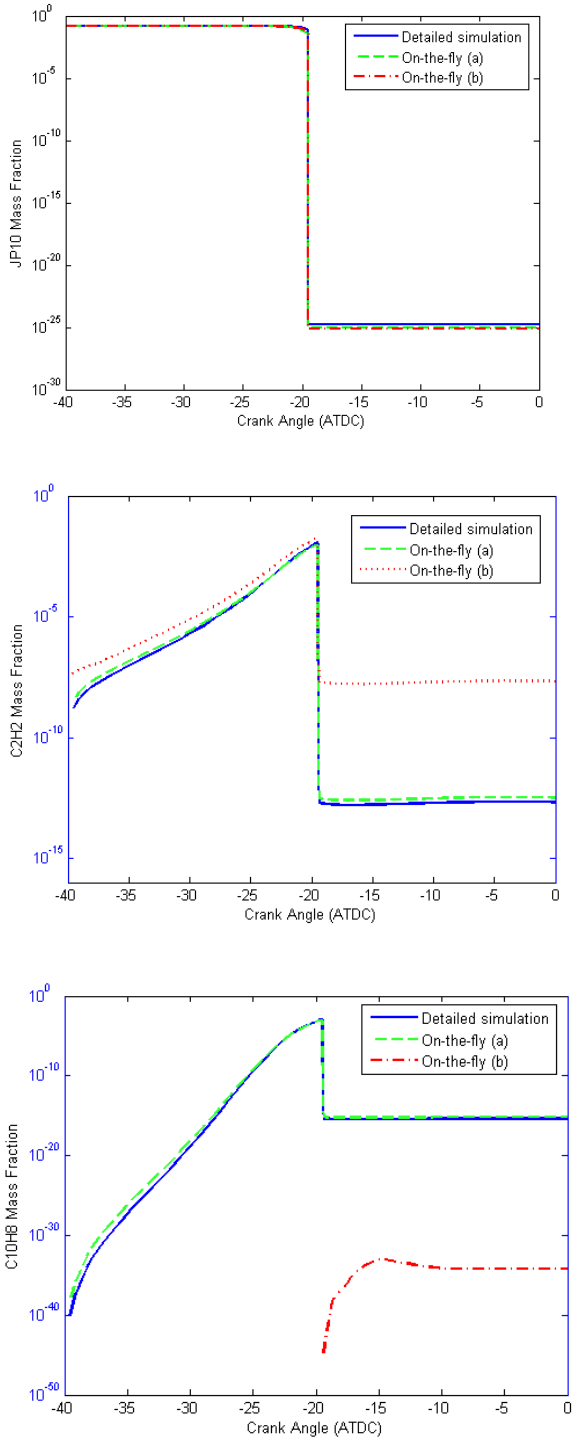

Figure 4.7: JP-10, C2H2, and C10H8 species mass fraction profiles of stoichiometric JP-10/air oxidation with soot formation in KIVA simulation. (a) soot formation separated from JP-10 oxidation, (b) soot formation not separated from JP-10 oxidation. Initial conditions: T=800 K, P=1 MPa.

Chapter 5

Kinetic Analysis Based on Element Flux

Complex kinetic mechanisms usually involve thousands of reactions and tens of thousands of reactions. In order to extract meaningful information from large mechanisms, advanced computational techniques will be required. In this work, a new program package has been created for the systematic kinetic analysis of complex reaction mechanisms. This program quantifies element transformation flux between species which provides a metric to evaluate the importance of species in the reaction network. Dynamic analysis of those flux values reveals the temporal evolution of the system. In addition to deriving the entire reaction network and capturing its dynamic evolution, a graph searching procedure is proposed to retrieve all possible reaction pathways from the highly complex reaction networks. Analysis of the flux involved in each pathway enables the quantification of pathway activity and allows both intra- and inter-system comparison of pathway importance. The approach is illustrated with detailed mechanisms describing n-pentane oxidation and methyl-butanoate oxidation.

5.1 Species analysis

The first level of kinetic analysis carried out by the program illustrates the importance of species in terms of sources and sinks in element transformation. Simply by sorting the pairs in descending order, we can identify leading transitions represented by large flux. If time-integrated flux data are examined, leading transitions reveal *globally* crucial species that play vital roles in the overall reaction process. On the other hand, if instantaneous

flux pointers are used, *locally* active species can be identified, representing local reaction characteristics. To better illustrate this idea, two mechanisms are analyzed in this section:

(1) Biodiesel surrogate methyl-butanoate mechanism (264 species and 1219 reactions) (Fisher, Pitz et al. 2000).

(2) N-pentane oxidation mechanism (385 species and 1895 reactions) (Curran 1998).

These two mechanisms are selected because they describe oxygenated fuel and hydrocarbon fuel oxidation respectively and the mechanisms are fairly large to demonstrate the capability of the analysis approach in retrieving meaningful kinetic information from complex mechanisms.

5.1.1 Global activity of species

A time-integrate flux analysis is performed in an adiabatic plug flow reactor (PFR) simulation. The calculations are performed using stoichiometric conditions at 650K and 950K to represent oxidation at low and high temperature (Androulakis 2004b; Curran 1998; Curran, Gaffuri et al. 1998). Table 5.1 summarizes the time-integrated carbon flux between species of methyl-butanoate and n-pentane oxidation. The first two columns represent the FROM and TO species of element transformation. The third column is the time-integrated flux data. Nearly two thousand source-sink connections have been identified for the entire mechanism. However, due to the space limitations, only species with large element flux are listed. Characteristic species of methyl-butanoate oxidation includes hydroperoxy alkylperoxy radical (MB2OOH4OO), cyclic ether (MBCY4O2), and methyl propenoate (MP2D). Hydroperoxy alkylperoxy radical (MB2OOH4OO) is formed by addition of a second oxygen molecule to the hydroperoxyalkyl radical (MB2OOH4J), which stems from initial radical (MB2J). The second oxygen addition to

initial radicals is a typical low temperature oxidation procedure (Fisher, Pitz et al. 2000). Cyclic ether MBCY4O2 is the product of decomposition of MB2OOH4J, which competes with second oxygen addition. Methyl propenoate MP2D is the product of beta scission of the carbon chain of methyl butanoate. It has the largest contribution to the original reactant oxidation. The identification of these source-sink connections in flux analysis reveals that there is competition between unimolecular decomposition and second oxygen addition in methyl butanoate oxidation. Another observation is that low temperature and high temperature oxidations of methyl butanoate have qualitatively very similar active species. However, the relative magnitude of element flux between sources and sinks establishes the fundamental difference between the two cases.

The flux analysis of n-pentane oxidation indicates that the shift between unimolecular decomposition and second oxygen addition as temperature increases is higher compared to methyl butanoate. At 650K, active species of n-pentane oxidation include hydroperoxy alkylperoxy radical C5H10OOH2-4O2, which is formed from second oxygen addition to hydroperoxyalkyl radical C5H10OOH2-4, cyclic ether C5H10O2-4, the product of C5H10OOH2-4 decomposition, and C3H6, from beta scission. However, as temperature increases to 950K, only species on beta scission pathways, e.g., C3H6, C2H5, etc., are identified. This almost complete shift from oxygen addition pathways to beta scission pathways as temperature increases indicates that the n-pentane oxidation pathways are more sensitive to temperature changes than methyl butanoate oxidation.

Table 5.1: Time-integrated carbon (C) flux of characteristic species in methyl butanoate and n-pentane oxidation at different initial temperatures. Carbon flux pointers are normalized to the largest pointer in the scheme to enable comparison between different schemes.

	Methyl butanoate			N-pentane		
	From	To	Relative C Flux	From	To	Relative C Flux
T_0=650K	CO	CO2	1.00E+00	CO	CO2	1.00E+00
	MP2D	C2H3CO	1.06E-02	CH3CO	CO	3.79E-02
	C2H2	HCCO	7.51E-03	NC5H12	C5H11-2	1.12E-02
	C2H3CO	C2H3	5.03E-03	C5H11-2	C5H11O2-2	4.88E-03
	MB2J	MP2D	1.97E-03	C5H11-2	C3H6	3.87E-03
	MB	MB2J	1.83E-03	C3H6	CH3CHCO	2.78E-03
	MB4OOH2J	MBCY4O2	1.79E-05	C5H11O2-2	C5H10OOH2-4	2.72E-03
	C3H6	C3H5-A	9.90E-06	C5H10OOH2-4O2	NC5KET24	1.93E-03
	MB2OOH4OO	MB4OOH2*O	6.88E-06	C5H10OOH2-4	C5H10OOH2-4O2	1.85E-03
	MB2OOH4J	MB2OOH4OO	5.83E-07	C5H10OOH2-4	C5H10O2-4	7.47E-04
T_0=950K	CO	CO2	1.00E+00	CO	CO2	1.00E+00
	MP2D	C2H3CO	1.95E-02	C2H2	HCCO	2.72E-01
	C2H3CO	CO	1.71E-02	C2H4	CH3	5.61E-02
	C3H5-A	C3H4-A	3.63E-03	C3H6	C3H5-A	2.07E-02
	MB	MB2J	3.51E-03	NC3H7	C2H4	4.56E-03
	MB2J	MP2D	2.89E-03	NC5H12	C5H11-2	4.14E-03
	MB2OOH4J	MBCY4O2	3.10E-05	C4H6	C2H4	4.13E-03
	MB2OO	MB2OOH4J	1.68E-06	C5H11-2	C3H6	2.69E-03
	MB2OOH4J	MB2OOH4OO	1.06E-07	C5H11-2	C2H5	1.79E-03
	MB2OOH4OO	MB2OOH2*O	8.20E-08	C5H11-1	NC3H7	1.14E-03

5.1.2 Local activity of species

Time-integrated flux identifies globally important species for the entire reaction process, compared with the instantaneous flux calculation that provides information about the specific stage of the oxidation process. Table 5.2 summarizes the instantaneous flux of methyl butanoate and n-pentane oxidations. As shown in Table 5.2, sources and sinks vary significantly at different stages of the oxidation process. For example, at the initial stage, fuel decomposition and oxidation are the main component of the combustion process. As the system proceeds, generation and oxidation of small species dominate the reaction process. When the system evolves to the final stage, the oxidation of very small species such as HCCO and CO becomes the dominant reactions.

Table 5.2: Instantaneous carbon (C) flux of methyl butanoate and n-pentane oxidation at different stages with initial temperature 650K.

	Methyl butanoate			N-pentane		
	From	To	C Flux	From	To	C Flux
Initial stage T=675K	MB2J	MB2OO	7.36E-01	C5H11-2	C5H11O2-2	8.34E+00
	MB	MB2J	7.06E-01	NC5H12	C5H11-2	8.30E+00
	MB3J	MB3OO	3.82E-01	C5H11O2-2	C5H10OOH2-4	4.19E+00
	MB	MB3J	3.74E-01	C5H10OOH2-4	C5H10OOH2-4O2	4.17E+00
	MB2O	C2H5CHO	2.76E-01	C5H11-3	C5H11O2-3	4.16E+00
	MB2OOH	MB2O	2.59E-01	NC5H12	C5H11-1	4.15E+00
	MB3OO	MB3OOH2J	2.48E-01	C5H11-1	C5H11O2-1	4.15E+00
	MB3OOH2J	MB2D	2.42E-01	NC5H12	C5H11-3	4.14E+00
	MB4J	MB4OO	2.27E-01	C5H10OOH2-4O2	NC5KET24	4.11E+00
	MB2OO	MB2OOH	2.05E-01	C5H10OOH2-4	C5H10O2-4	2.00E+00
Intermediate stage T=1550K	HCO	CO	1.12E+03	HCO	CO	9.75E+02
	CH2O	HCO	8.52E+02	CH2O	HCO	7.51E+02
	MB2D	C5H7O2	4.08E+02	C3H6	C3H5-A	4.32E+02
	CH3O	CH2O	4.00E+02	C3H5-A	C3H5O	3.32E+02
	C5H7O2	CH2CHCHCO	3.89E+02	CH3CO	CO	2.99E+02
	MP2D	C2H3CO	3.63E+02	CH3CHO	CH3CO	2.89E+02
	C2H3O1,2	CH3CO	3.02E+02	CH3CO	CH3	2.84E+02
	CH2CHO	C2H3O1,2	2.97E+02	C2H5	C2H5O	2.70E+02
	C2H3CO	C2H3	2.88E+02	C2H3O1,2	CH3CO	2.65E+02
	CH3CO	CO	2.25E+02	CH2CHO	C2H3O1,2	2.60E+02
Final stage T=2550K	CO	CO2	3.50E+04	CO	CO2	5.05E+04
	SC3H5OCH2	C3H5-S	2.51E+03	HCO	CO	2.46E+04
	C3H5-S	C3H4-P	2.05E+03	CH2O	HCO	2.08E+04
	HCO	CO	1.63E+03	CH3	CH2O	1.35E+04
	CH2O	HCO	1.50E+03	C2H2	HCCO	1.20E+04
	C3H4-P	C3H3	1.38E+03	CH4	CH3	8.91E+03
	C3H3	C3H2	1.14E+03	HCCO	CO	8.54E+03
	HCCO	CO	9.61E+02	C2H3	C2H2	6.68E+03
	C2H2	HCCO	9.23E+02	C2H4	C2H3	5.31E+03
	SC3H5OCH2	CH2O	8.37E+02	HCCO	CH2(S)	4.38E+03

5.2 Pathway analysis

Another valuable output of the program is the identification of individual pathways and the quantification of their activities. The element flux indicators provided by flux analysis describe the transition between two species, and illustrate important connections between fuels and final products. Given this information between sources and sinks, a Breadth First Search (BFS) algorithm (Dixon 1998) can be employed to identify the reaction pathways. The BFS algorithm initiates from initial species (e.g., fuels) and find all species that are connected to the initial species. These newly found species are stored in

the algorithm as second level species, which serves as initial species in the next searching step. The search algorithm repeats the breadth first searching until no further species can be identified. An illustrative example of pathway identification is given in Figure 5.1, where all possible pathways are identified based on the connection information between species and visualized in a flux graph. Note that since this example is shown for illustration purposes only, material balances are not enforced in this system.

	FROM	TO	Flux
1	A	B	150
2	A	C	200
3	A	F	50
4	B	D	5
5	B	E	8
6	C	D	1
7	D	E	3
8	D	F	2
9	E	F	10

	Pathways
1	ABDF
2	ACDF
3	ABDEF
4	ACDEF
5	ABEF
6	AF

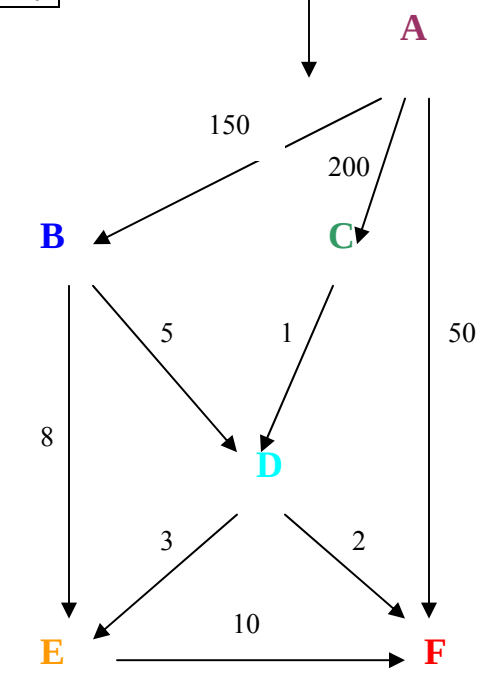

Figure 5.1: Pathway identification and visualization based on element flux indicators.

The pathways identified from flux analysis provide qualitative connections between reactants and products. However, to analyze pathway activities, a quantitative procedure needs to be developed. Based on the flux analysis, we propose to use the normalized flux values to quantify the weight of each pathway. In the proposed method, the influx/outflux of each species from/to different species are normalized to the total influx/outflux of this species to evaluate the contribution of each connection. Taking the system in Figure 5.1 for example, when the consumption pathways of A is examined, the calculation initiates from A and all its outflux connections, AB, AC, and AF, are normalized to the total out flux of species A (400), which gives the weight of each connection as shown in Figure 5.2 (a). Then the calculation proceeds to species B, C, and F. The two outflux connections of species B (BE and BD) are normalized to the total out flux of B (13), while the only outflux from C (CD) is given the weight of 1. Since F does not have outflux connection, no outflux normalization is needed. The normalization procedure then proceeds until no further outflux connection is found. On the other hand, if the production pathways of F is to be analyzed, the calculation initiates from F and all its influx connects are normalized. Three influxes of F can be identified in the system, and they are normalized to the total influx of F (62), giving normalized weight as shown in Figure 5.2 (b). The normalization procedure proceeds until no further influx can be identified.

Table 5.3: Scaled pathway weights of the system shown in Figure 5.1.

	Pathways	Weights of pathways from A	Weights of pathways to F
1	ABDF	5.78%	2.49%
2	ACDF	20.00%	0.51%
3	ABDEF	8.66%	3.59%
4	ACDEF	30.00%	0.73%
5	ABEF	23.06%	11.68%
6	AF	12.50%	81.00%
Total		100.0%	100.0%

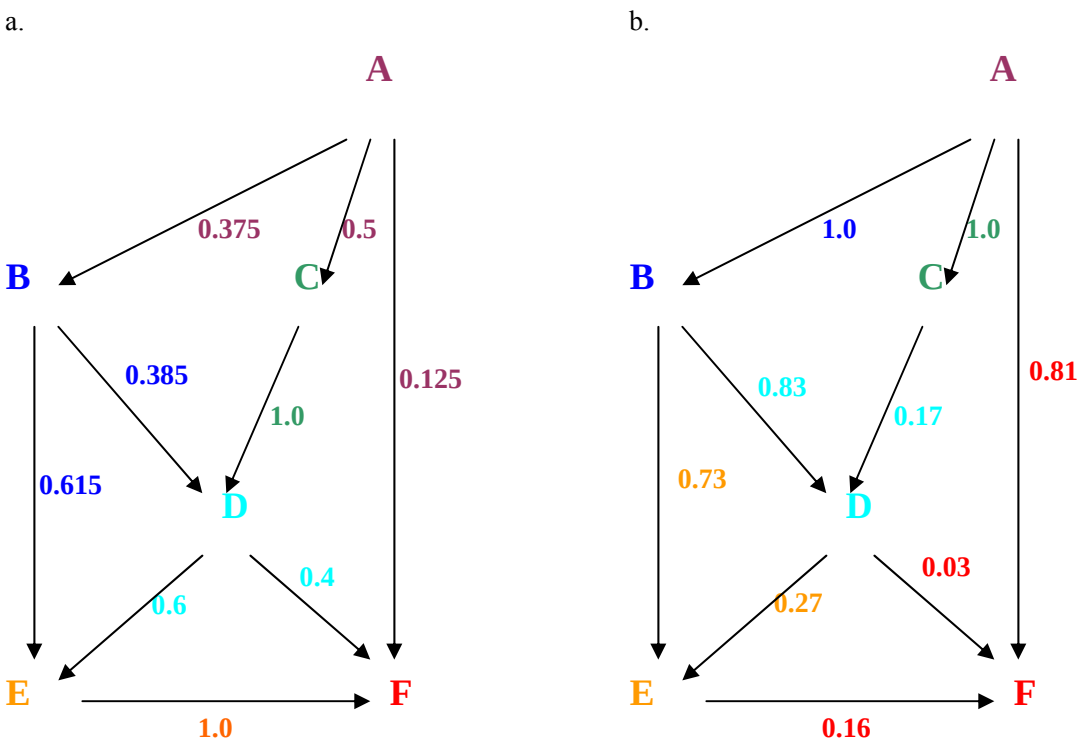

Figure 5.2: Flux normalization procedure to calculate pathway activity. (a) outflux of species on pathways from species A are normalized, and (b) influx of species on pathways to species F are normalized.

Table 5.4: Characteristic pathways of methyl butanoate and n-pentane combustion.

	Pathway	Scaled pathway weight	
		T_0=650K	T_0=950K
Methyl butanoate	MB → MB2J → MP2D → C2H3CO → C2H3 → C2H2 → HCCO → CO → CO2	46.19%	46.74%
	MB → MB2J → MB2OO → MB2OOH4J → MB2OOH4OO → MB4OOH2*O → MP3J2*O → CH3OCO → CH3O → HCO → CO → CO2	10.22%	3.01%
	MB → MB2J → MB2OO → MB2OOH4J → MBCY4O2 → MP2D → C2H3CO → C2H3 → C2H2 → HCCO → CO → CO2	7.31%	4.12%
	MB → MBMJ → NC3H7CO → NC3H7 → C2H4 → C2H3 → C2H2 → HCCO → CO → CO2	6.83%	8.88%
	MB → MBMJ → MBMOO → MBMOOH2J → MBCY2OM → SC3H5OCH2 → C3H5-S → C2H2 → HCCO → CO → CO2	5.38%	3.17%
N-pentane	NC5H12 → C5H11-2 → C5H11O2-2 → C5H10OOH2-4 → C5H10OOH2-4O2 → NC5KET24 → CH3COCH2 → CH2CO → HCCO → CO → CO2	15.96%	0.32%
	NC5H12 → C5H11-2 → C3H6 → C3H5-A → C3H4-A → C3H3 → C3H2 → HCCO → CO → CO2	37.88%	81.12%
	NC5H12 → C5H11-2 → C5H11O2-2 → C5H10OOH2-4 → C5H10O2-4 → CH3CO → CO → CO2	27.16%	1.01%

After the weight of each connection is calculated, pathway weights are obtained by multiplying each connection weight. When consumption pathways, i.e., pathways *from* certain species, are examined, normalized outflux values of species on the pathway are multiplied. When production pathways, i.e., pathways *to* specific species, are evaluated, normalized influx values of the species on the pathway are used in multiplication. Scaled pathway weights of the system in Figure 5.1 are shown in Table 5.3. The scaled pathway weights can be interpreted in the following ways: scaled weights of pathways from certain species measure the contribution of each pathway to the consumption of this specific species, while scaled weights of pathways to certain species weigh the contribution of each pathway to the production of this specific species. Thus for the example considered in Figure 5.1, the pathway activity in Table 5.3 can be interpreted in the following way. Pathway ACDEF makes the largest contribution to the consumption of species A and has a weight of 30%, while pathway AF is the most important pathway in the production of species F with an 80% contribution. The pathway weights calculated in this method are normalized to the value of 1, which enables direct comparison of pathway activity between different systems.

To demonstrate the pathway analysis method in complex kinetic mechanisms, the proposed method is applied on the methyl butanoate and n-pentane mechanisms. In the searching step, methyl butanoate and n-pentane are considered as initial species to analyze fuel oxidation pathways. 356 key pathways are identified for n-pentane oxidation and 293 key pathways for methyl-butanoate in the searching procedure. Due to the limitations of space, only a few characteristic pathways are summarized in Table 5.4. The contribution of different pathways to the oxidation of original reactants can be interpreted

from the pathway activities. The pathways summarized in Table 5.4 involve various regimes such as second oxygen addition, hydroperoxyalkyl radical decomposition, and beta scission. Based on the results shown in Table 5.4, it is found that the preferential oxidation pathway of methyl butanoate is through the hydrogen abstraction from the carbon chain (pathways 1-3) rather than the methoxyl group (pathways 4 and 5). At both temperatures (650K and 950K) the combined contribution of pathways from hydrogen abstraction on the carbon chain (63.72% at 650K and 53.87% at 950K) are much larger than that of pathways from hydrogen abstraction on the methoxyl group (12.21% at 650K and 12.05% at 950K). Lacking an ester group, n-pentane has less complicated oxidation pathways. At 650K, three major pathways are identified, with beta scission the most important (37.88%), followed by second oxygen addition (15.96%) and hydroperoxyalkyl decomposition (27.16%). The competition favors beta scission as the temperature increases. The scaled pathway weights indicate that beta scission accounts for 81.12% of n-pentane oxidation at 950K while second oxygen addition and hydroperoxyalkyl decomposition exhibit very small activities (0.32% and 1.01%).

5.3 Reactivity Index: a compact representation of chemical status

Based on temperature, pressure, and species compositions, element fluxes can be evaluated, which can be further used to derive pathway weights. Thus, the chemical status of each computational cell at each time step can be fully captured by any of these three categories of parameters. However, for a complex kinetic mechanism which involves thousands of reacting species and tens of thousands of reactions, representation of chemistry by any of these three approaches is too expensive to compute, store, and interpret due to the fact that for every computational unit (time step and computational

cell) a multi-dimensional vector is needed. In order to represent, analyze and visualize effectively the chemical status of the system, we introduce a novel approach that arrives at a compact representation of the information content of these multi-dimensional vectors. This approach allows the projection of the totality of the information contained in temperature, pressure, species compositions, element fluxes, or pathway weights onto a single scalar. In doing so, multi-dimensional data can be first streamed from the temporally and spatially evolving chemical system, and these data are further processed and assigned a scalar "reactivity index". These reactivity indexes allow quick identification of the chemical status of the system at different time points and/or geometric regions.

In order to convert multi-dimensional data to scalar reactivity indexes, we employ cosine coefficient, which was previously introduced in Chapter 2 to perform graph clustering, to do the projection. The metric based on cosine coefficient provides a normalized measure for similarity between two multi-dimensional vectors, thus it is widely used in data mining and clustering (Schultz and Liberman 1999; Tan 2005). This cosine coefficient metric evaluates the similarity between any two vectors with same number of dimensions. Therefore a base vector with all dimensions to be unity is used to assign each multi-dimensional vector a cosine coefficient. During a reactive simulation, temperature, pressure, and species compositions, or element fluxes, or pathway weights are steamed from reactive flow simulations as "pseudo time series" evolving in time and space. Then for each of the streamed multi-dimensional vector, its cosine similarity between the base vector is calculated and assigned to current system state. The outcome of this process is an integer representing the local chemical status of the reaction system.

Given this cosine similarity projection method, another question remains. That is, which group of data should be used to perform this calculation? Based on our previous demonstration that element fluxes can better capture the chemical status than temperature, pressure, and species compositions (Androulakis 2004b), we can narrow the choice to element fluxes, and pathway weights which are derived based on element fluxes. Figure 5.3 compares cosine coefficient calculated based on fluxes and pathway weights during n-heptane combustion in a PFR model. It can be noticed that cosine coefficient of pathway weights are more spread out than that of original fluxes. This is due to the fact that in original flux, a few species pairs such as CO to CO_2 have much larger flux than other species, which makes these few species dominant in the cosine coefficient calculation. While in pathway weights, since outflux or influx of each species are normalized (refer to Section 5.2 for details), the impact of large fluxes are eliminated through normalization. Therefore, cosine coefficient based on pathway weights better distinguishes the difference between two system states, and thus better serves our purpose to derive a reactivity index to represent chemical status.

This reactivity index calculation is performed for HCCI engine combustion simulated in KIVA-3V. A reactivity index is derived for each computational cell at each time step. Reactivity indexes of the chamber at different time steps are shown in Figure 5.4. An idealized case is used in this study, with initial temperature ranging from 750K to 1100 K and initial equivalence ratio ranging from 0.2 to 1.6. During compression, cool flame behavior was observed at region 3 which corresponds to initial temperature 750K. Fuel was consumed and temperature was increased to similar level of region 2. This cool flame behavior is well captured by the reactivity index: reactivity index at this region is

much larger than the rest part of the chamber. Another observation from the reactivity index is that regions with the same initial temperature have similar reaction status than two regions with the same equivalence ratio. Taking regions 2, 3, and 4 for example, region 2 and region 3 have the same equivalence ration but different initial temperatures while region 3 and region 4 have the same initial temperature but different equivalence ratios. As indicated by the reactivity index, region 3 and region 4 are more similar than region 2 and region 3. This is demonstrated by pathway analysis for these three regions. Leading pathways and their weights at these three regions are compared in Table 5.5. The results indicate that region 3 and region 4 have very similar leading pathways, while region 2 have a different set of active pathways.

When the chamber is ignited and the flame propagates, reactivity index divides the chamber into four regions. A thin region with the largest reactivity index is the flame front. In front of flame front is the un-ignited region which has elevated reactivity index and is ready to be ignited. Right behind the flame front is the post-ignition region where some remainder oxidation reactions are taking place. Behind the post-ignition region is the area where ignition is complete and all reactions are finished, resulting in lowest reactivity index. This chemical status information can not be interpreted from other parameters such as temperature and n-heptane concentration.

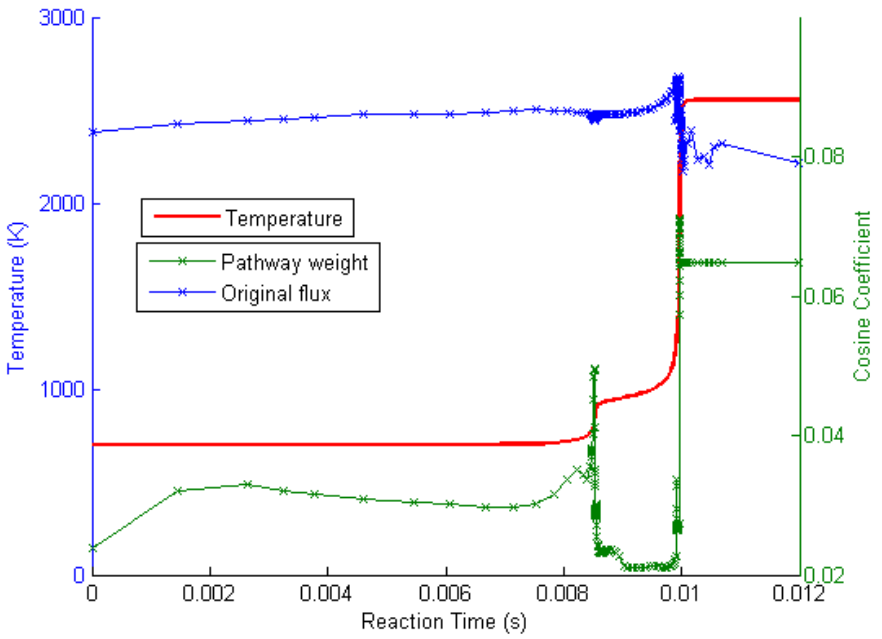

Figure 5.3: Cosine coefficient calculated based on pathway weights and original fluxes. Data obtained for n-heptane oxidation in a PFR model. Initial temperature: 750K; equivalence ratio: 1.0.

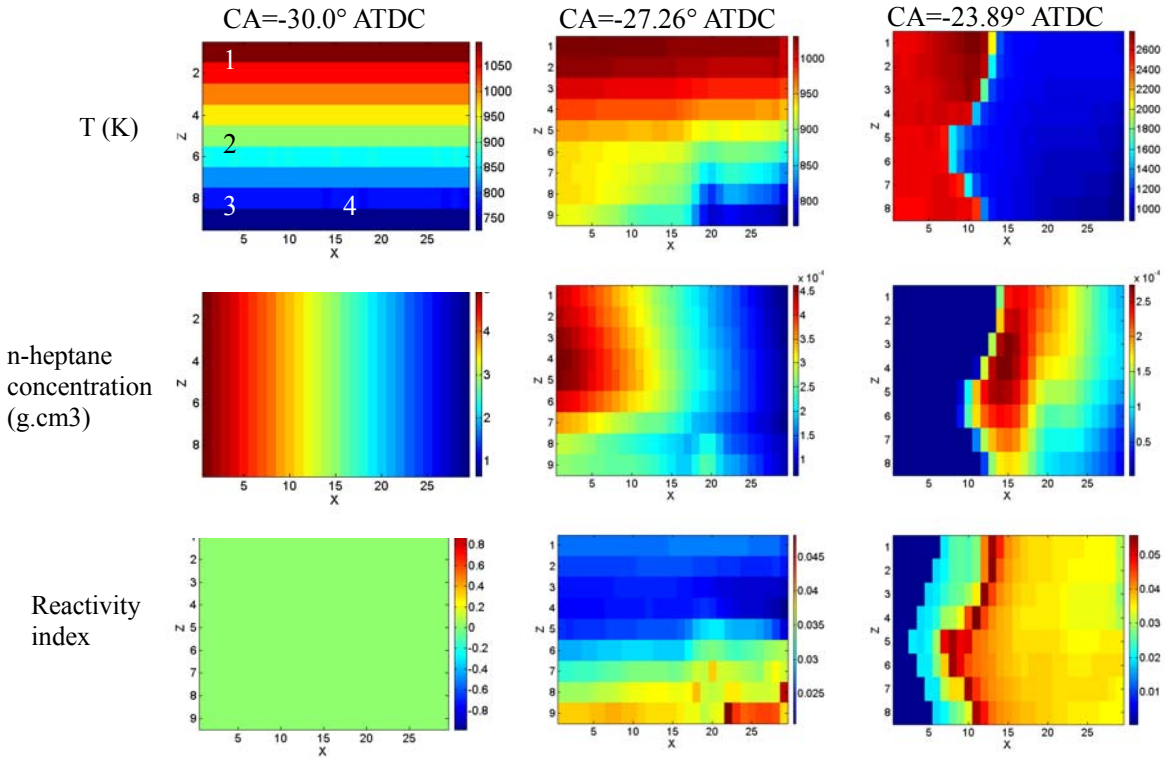

Figure 5.4: Temperature, n-heptane concentration, and reactivity index in HCCI engine chamber simulated in KIVA-3V.

Table 5.5: Leading pathways of different regions in HCCI engine chamber at CA=-27.26° ATDC.

	Pathway	Pathway weight
Region 2	NC7H16 → C7H15-1 → C7H15O2-1 → C7H14OOH1-4 → C7H14O1-4 → CH2CHO → CH3CO → CO → CO2	5.71%
	NC7H16 → C7H15-2 → C5H11-1 → C2H4 → HCO → CO → CO2	4.89%
	NC7H16 → C7H15-2 → C7H15O2-2 → C7H14OOH2-5 → C7H14O2-5 → CH3COCH2 → CH2CO → HCCO → CO → CO2	4.16%
Region 3	NC7H16 → C7H15-2 → C7H15O2-2 → C7H14OOH2-4 → C7H14OOH2-4O2 → NC7KET24 → NC3H7CHO → NC3H7 → CH3 → CH2O → HCO → CO → CO2	2.08%
	NC7H16 → C7H15-1 → C7H15O2-1 → C7H14OOH1-4 → C7H14O1-4 → CH2CHO → CH3CO → CO → CO2	1.55%
	NC7H16 → C7H15-3 → C7H15O2-3 → C7H14OOH3-5 → C7H14OOH3-5O2 → NC7KET35 → C2H5 → C2H4 → HCO → CO → CO2	1.37%
Region 4	NC7H16 → C7H15-1 → C7H15O2-1 → C7H14OOH1-4 → C7H14O1-4 → CH2CHO → CH3CO → CO → CO2	1.87%
	NC7H16 → C7H15-2 → C7H15O2-2 → C7H14OOH2-4 → C7H14OOH2-4O2 → NC7KET24 → NC3H7CHO → NC3H7 → CH3 → CH2O → HCO → CO → CO2	1.48%
	NC7H16 → C7H15-3 → C7H15O2-3 → C7H14OOH3-5 → C7H14OOH3-5O2 → NC7KET35 → C2H5 → C2H4 → HCO → CO → CO2	1.32%

5.4 Summary

This paper presented a computer program that performs fundamental kinetic analysis of complex reaction mechanisms based on time-integrated and instantaneous element flux. The flux pointers are used for the analysis of species activities, correlation between species activity and system dynamics, pathways activities, and representation of chemical status using a reactivity index. Four novel aspects of this flux-based kinetic analysis program are illustrated:

(1) The program analyzes species activities based on element flux which provides

accurate representation of reactive propensity.

(2) The analysis enables automatic identification of pathways connecting specific species in the system. The coupling of flux analysis and graph visualization software allows the visual inspection of the reaction pathways.

(3) By employing a normalized in-flux and out-flux of each species in the pathway, the program is able to quantify the activity of the entire pathway.

(4) By comparing the pathway weights vector to a base vector, a compact representation of chemical status is assigned to the temporally and spatially evolving reaction system.

The program has been designed to be a stand alone package which is readily to be extended to other applications that involve graph and pathway components. By optimizing the flux computing algorithm, the CPU required for the analysis is reduced to a minimal level, which makes it easy to interface this program to other simulation programs.

Chapter 6

Conclusions and Future Perspectives

6.1 Summary

In this dissertation, a novel graph-based adaptive mechanism reduction approach is proposed first to adaptively address different reaction conditions in reactive flow simulations. Element flux is employed in the reduction methods to describe the reaction system and develop adaptive reduced mechanisms, instead of the temperature, pressure and species composition commonly used in conventional approaches. An efficient search algorithm is developed to accommodate the adaptive scheme in a flow calculation. Rather than searching among all the data points in the training set, cluster centers are used to represent the clusters and assign new query points proper mechanisms. Reduced mechanisms are developed by setting a high portion cutoff to instantaneous fluxes, which is simple to realize, yet effectively captures the most active species and reactions in the reaction system. By verifying in a PMSR and a PFR model, it is demonstrated that reduced mechanisms developed under this methodology can predict the temperature, species composition and auto ignition delay with excellent agreement to detailed simulations. Meanwhile, simulation CPU time is largely reduced.

High fidelity is observed from the adaptive scheme and CPU time is tremendously reduced. However, several shortcomings have limited the validity of this adaptive scheme. Firstly, the adaptive scheme relies on a library of reduced mechanisms developed beforehand, and it's based on the assumption that the feasible regions of these reduced

mechanisms can cover the entire condition space. When conditions confronted in combustion processes are beyond the feasible regions of these reduced mechanisms, the library becomes insufficient. Thus in our later work, an on-the-fly mechanism reduction approach is proposed to analyze and reduce complex kinetic mechanisms dynamically within the context of reactive flow simulations. No *apriori* information or analysis is necessary for the on-the-fly approach. Furthermore, any condition encountered in the flow simulation can be addressed appropriately. This feature of the on-the-fly scheme enables its implementation in reactive flow simulations when no *apriori* information is available for the accessible condition space. In addition to its adaptability, the on-the-fly scheme it self can be performed with minimal CPU overhead. This enables its integration in each computational cell and time step of complex CFD models.

The on-the-fly scheme is demonstrated in zero-dimensional flow models such as PMSR and PFR, and a complex engine CFD code KIVA-3V. Good agreement has been observed between on-the-fly simulation results, detailed simulation results, and experimental data. On the computational efficiency side, CPU time is reduced by a factor up to 20 in the CFD code we examined.

In addition to fuel chemistry, pollutant formation, including NOx and soot, is another major part of combustion simulations. To incorporate NOx and soot formation in reduced mechanisms, a novel multi-element flux analysis approach and a graph-searching procedure were introduced in the reduction scheme. In the multi-element flux analysis, nitrogen flux exclusively captures NOx formation chemistry, while carbon, hydrogen, and oxygen transitions effectively characterize fuel oxidation network. The graph searching procedure considers CO_2 and soot precursor PAHs (poly aromatic

hydrocarbons) as roots of fuel oxidation network and soot formation network, respectively, and searches reversely through the carbon element transition network to separate two reaction networks. Given the separated fuel oxidation and soot formation networks, flux analysis is employed on each network to identify their respective active species, which are then combined to define the reduced mechanism. The multi-element flux analysis with graph searching procedure incorporates both fuel oxidation and pollutant formation in CFD calculations, which facilitates more comprehensive study of combustion systems.

Element flux analysis not only can be used as a metric to reduce kinetic mechanisms, it also provides useful information about the kinetic system to perform systematic kinetic analysis. In this dissertation, a new program package is created for the systematic kinetic analysis of complex reaction mechanisms, including the features of dynamic active species identification, principal elemental transformation network derivation, and independent pathway analysis. The program retrieves data from CHEMKIN based simulation programs and calculates element transformation flux from reactants to intermediates and finally products over specific time intervals. Based on the element flux calculation, the program carries out two types of kinetic analysis targeting at species and pathways, respectively. The species analysis identifies important species over the entire process or within specific time interval. In addition, by tracing the influx and/or outflux of each species, the behavior of individual species can be correlated to the evolution of the entire system. This facilitates the investigation of species that are representative to specific system behaviors. Another feature of this program is the identification of pathways from the complex reaction network and evaluation of their activities at different

regimes. A graph searching technique is employed to retrieve pathways between given species and a weight propagation procedure is introduced to quantify the importance of each pathway on a normalized scale. This allows the quantification of contributions of different pathways to the system as well as the comparison of pathways between different systems. The reactivity index derived based on pathway weights provides a compact representation of chemical status. This derivation of reactivity index allows the projection of the totality of the information contained in high dimensional pathway weights onto a single scalar. In doing so, multi-dimensional data can be first streamed from the temporally and spatially evolving chemical system, which are further processed and assigned a scalar "reactivity index" to each vector. These reactivity indexes allow quick identification of the chemical status of the system at different time points and/or geometric regions.

6.2 Future work

One of the key contributions of the proposed on-the-fly reduction framework is to integrate complex kinetic mechanisms in realistic flow simulations. Thus in our future work, we will explore the combustion characteristics of fuels that involve highly complex kinetics which is can not be accommodated by conventional approaches. Of particular interest are biofuels which have drawn rapidly growing attention due to its renewable nature and environmental benefits.

Although there is a dramatic increase in biofuels production and related research, few studies have been focused on the investigation of biofuels combustion using detailed kinetics. This is mainly due to the fact that biofuels are usually multiple-component mixtures which make it very challenging to develop surrogate reaction mechanisms; and

detailed mechanisms are usually too complex to be incorporated in reactive flow calculations.

The work in this dissertation resulted in the development of an on-the-fly chemistry framework based on element flux analysis that captures local reactive propensity with great accuracy while reduces computational intensity. The emphasis of our future work is the characterization of biofuel combustion and integration with advanced flow models using an advancement of the on-the-fly kinetic representation.

In particular there are three specific aims that worth our further attention in the future work. The first aim is the kinetic analysis of biofuel combustion and pollutant formation where element flux analysis is used to characterize biofuel oxidation, pollutant formation, and interaction with fossil fuels and commercial additives. The second aim is the development of an advanced on-the-fly representation framework that enables the detailed analysis of complex kinetic networks such as the ones developed for biofuels combustion. The on-the-fly representation framework is designed to takes advantages of parallel computing and other computational approaches. The completion of these two tasks gives rise to a kinetic analysis framework which enables the characterization of biofuel combustion based on detailed kinetic models. In the third specific aim, the framework is integrated in CFD codes to incorporate complex biofuel kinetics in realistic flow calculation in order to characterize biofuel performance in engine combustion.

Another direction of our future work would be further optimization of the on-the-fly reduction framework. One approach that worth pursuing is to combine this flux-based reduction method which mainly focuses on the reduction of mechanism size with other approaches that target the removal of stiffness of the kinetic system. A good example is to

combine quasi-steady species approximation (QSSA) with flux-based mechanism reduction. The main challenge in this direction is the overhead introduced by stiffness evaluation in addition to element flux analysis. Thus our task on this direction is to arrive at an efficient way to remove stiffness dynamically during the simulation. Successful combination of mechanism size reduction (flux-based approach) and stiffness removal could significantly improve the speed of realistic flow simulations with detailed chemistry.

Bibliography

Abraham, J.a.B., F. V., 1989. Fuel-air mixing and distribution in a direct-injection stratified-charge rotary engine. Society of Automotive Engineers Technical Paper 890329.

Aceves, S.M., Flowers, D.L., Westbrook, C.L., Smith, J.R., Pitz, W., Dibble, R., Christensen, M., Johansson, B., 2000. A Multi-zone Model for Prediction of HCCI Combustion and Emissions. SAE paper 2000-01-0327.

Amsden, A.A., 1997. KIVA-3V: A Block-Structured KIVA Program for Engines with Vertical or Canted Valves. . Los Alamos National Laboratory Report LA-13313-MS.

Androulakis, I.P., 2000. Kinetic mechanism reduction based on an integer programming approach. Aiche Journal **46**(2): 361-371.

Androulakis, I.P., 2004a. "Store and retrieve" representations of dynamic systems motivated by studies in gas phase chemical kinetics. Computers & Chemical Engineering **28**(11): 2141-2155.

Androulakis, I.P., 2006. New approaches for representing, analyzing and visualizing complex kinetic transformations. Computers & Chemical Engineering **31**(1): 41-50.

Androulakis, I.P., Grenda, J. M., Bozzelli, J. W., 2004b. Time-integrated pointers for enabling the analysis of detailed reaction mechanisms. Aiche Journal **50**(11): 2956-2970.

Arya, S., Mount, D.M., Netanyahu, N.S., Silverman, R.Wu, A.Y., 1998. An optimal algorithm for approximate nearest neighbor searching in fixed dimensions. Journal of the Acm **45**(6): 891-923.

Babajimopoulos, A., Assanis, D.N., Flowers, D.L., Aceves, S.M., Hessel, R.P., 2005. A Fully Integrated CFD and Multi-zone Model with Detailed Chemical Kinetics for the Simulation of PCCI Engines. 15th International Multidimensional Engine Modeling Users' Group Meeting, Detroit, MI, USA.

Banerjee, I.Ierapetritou, M.G., 2003. Development of an adaptive chemistry model considering micromixing effects. Chemical Engineering Science **58**(20): 4537-4555.

Bhattacharjee, B., Schwer, D.A., Barton, P.I.Green, W.H., 2003. Optimally-reduced kinetic models: reaction elimination in large-scale kinetic mechanisms. Combustion and Flame **135**(3): 191-208.

Bruno, T.J., Marcia L. Huber, Arno Laesecke, Eric W. Lemmon, Richard A. Perkins. 2006. Thermochemical and Thermophysical Properties of JP-10, National Institute of Standards and Technology.

Chen, J.Y., 1988. A general procedure for constructing reduced reaction mechanisms with given independent reactions. Combustion Science Techniques **57**: 89-94.

Chiang, C.H., Raju, M.S.Sirignano, W.A., 1992. Numerical-Analysis of Convecting, Vaporizing Fuel Droplet with Variable Properties. International Journal of Heat and Mass Transfer **35**(5): 1307-1324.

Choi, G.H., Han, S.B.Dibble, R.W., 2004. Experimental study on homogeneous charge compression ignition engine operation with exhaust gas recirculation. International Journal of Automotive Technology **5**(3): 195-200.

Curran, H.J., Gaffuri, P., Pitz, W.J.Westbrook, C.K., 1998. A comprehensive modeling study of n-heptane oxidation. Combustion and Flame **114**(1-2): 149-177.

Curran, H.J., P. Gaffuri, W.J. Pitz, C. K. Westbrook, C. V. Callahan, and F. L. Dryer 1998. Oxidation of Automotive Primary Reference Fuels at Elevated Pressures. Twenty-seventh Symposium (International) on Combustion, Boulder, CO.

Dec, J.E., 2009. Advanced compression-ignition engines-understanding the in-cylinder processes. Proceedings of the Combustion Institute **32**: 2727-2742.

Dibble, R.W., M. Au, J.W. Girard, S.M. Aceves, D.L. Flowers, J.M. Frias. 2001. A review of HCCI engine research: analysis and experiments. SAE paper 2000-01-2511.

Dixon, C., 1998. Temporal resolution using a breadth-first search algorithm. Annals of Mathematics and Artificial Intelligence **22**(1-2): 87-115.

Fansler, T.D., Drake, M.C., Gajdeczko, B., Duwel, I., Koban, W., Zimmermann, F.P.Schulz, C., 2009. Quantitative liquid and vapor distribution measurements in evaporating fuel sprays using laser-induced exciplex fluorescence. Measurement Science & Technology **20**(12): -.

Faravelli, T., Antichi, A., Callierotti, C., Ranzi, E.Benedetto, D., 1997. A kinetic study of an advanced reburning process. Combustion Theory and Modelling **1**(4): 377-393.

Faravelli, T., Bua, L., Frassoldati, A., Antifora, A., Tognotti, L.Ranzi, E., 2001. A new procedure for

predicting NOx emissions from furnaces. Computers & Chemical Engineering **25**(4-6): 613-618.
Fieweger, K., Blumenthal, R., Adomeit, G., 1997. Self-ignition of SI engine model fuels: A shock tube investigation at high pressure. Combustion and Flame **109**(4): 599-619.
Fisher, E.M., Pitz, W.J., Curran, H.J.Westbrook, C.K., 2000. Detailed chemical kinetic mechanisms for combustion of oxygenated fuels. Proceedings of the Combustion Institute **28**: 1579-1586.
Flowers, D.L., S.M. Aceves, J.R. Smith, J. Torres, J. Girard, R.W. Dibble. 2000. HCCI in a CFR Engine: Experiments and Detailed Kinetic Modeling. SAE paper 2000-01-0328.
Gansner, E., Koutsofios, E.North, S., 2006. Drawing graphs with dot. dot User's Manual**:** 2-4.
Granata, S., Faravelli, T., Ranzi, E., Olten, N.Senkan, S., 2002. Kinetic modeling of counterflow diffusion flames of butadiene. Combustion and Flame **131**(3): 273-284.
Griffiths, J.F., 1995. Reduced Kinetic-Models and Their Application to Practical Combustion Systems. Progress in Energy and Combustion Science **21**(1): 25-107.
He, K., Marianthi G. Ierapetritou, Ioannis P. Androulakis. 2008. A graph-based approach to developing adaptive representations of complex reaction mechanisms Combustion and Flame **155**(4): 585-604.
Hirschfelder J.O., C.C.F., 1949. Theory of propagation of flames. 3rd Symp. Comb, Flame and Explosion Phenomena, Baltimore.
Hou, Z.-X.a.A., J., 1995. Three-dimensional modeling of soot and NO in a direct-injection diesel engine. Society of Automotive Engineers Technical Paper 950608.
Hsieh, S.H., Paulino, G.H.Abel, J.F., 1995. Recursive Spectral Algorithms for Automatic Domain Partitioning in Parallel Finite-Element Analysis. Computer Methods in Applied Mechanics and Engineering **121**(1-4): 137-162.
J. Wei, J.K., 1969. A lumping analysis in monomolecular reaction systems. Analysis of exactly lumpable systems. Industrial & Engineering Chemistry Fundamentals **8**(1): 114-123.
Jardine, N., and Sibson, R., 1968. Construction of hierarchical and nonhierarchical classifications. Computer Journal **13**: 116-117.
Jiang, Y., Qiu, R.Fan, W.C., 2005. A kinetic modeling study of pollutant formation in premixed hydrocarbon flames. Chinese Science Bulletin **50**(3): 276-281.
Jones, W.P., Whitelaw, J.H., 1985. Modelling and measurement in turbulent combustion. 20th Symp Comb, Pittsburgh.
Kanungo, T., Mount, D.M., Netanyahu, N.S., Piatko, C.D., Silverman, R.Wu, A.Y., 2002. An efficient k-means clustering algorithm: Analysis and implementation. Ieee Transactions on Pattern Analysis and Machine Intelligence **24**(7): 881-892.
Karypis, G., 2002. CLUTO - A Clustering Toolkit. Computer Science and Engineering Technical Report Abstract, University of Minnesota.
Karypis, G.Kumar, V., 1998a. Multilevel k-way partitioning scheme for irregular graphs. Journal of Parallel and Distributed Computing **48**(1): 96-129.
Karypis, G.Kumar, V., 1998b. A fast and high quality multilevel scheme for partitioning irregular graphs. Siam Journal on Scientific Computing **20**(1): 359-392.
Kee, R.J., Rupley, F.M., Meeks, E., Miller, J.A. . 1996. CHEMKIN-III: A FORTRAN chemical kinetics package for the analysis of gas-phase chemical and plasma kinetics. Livermore, CA (United States), Sandia National Labs.
Kim, D.S.Lee, C.S., 2006. Improved emission characteristics of HCCI engine by various premixed fuels and cooled EGR. Fuel **85**(5-6): 695-704.
Kong, S.C.Reitz, R.D., 2003a. Application of detailed chemistry and CFD for predicting direct injection HCCI engine combustion and emissions. Proceedings of the Combustion Institute **29**: 663-669.
Kong, S.C.Reitz, R.D., 2003b. Numerical study of premixed HCCI engine combustion and its sensitivity to computational mesh and model uncertainties. Combustion Theory and Modelling **7**(2): 417-433.
Lam, S.H., Goussis, D. A., 1994. The Csp Method for Simplifying Kinetics. International Journal of Chemical Kinetics **26**(4): 461-486.
Law, D., Kemp, D., Allen, J., Kirkpatrick, G., Copland, T., 2001. Controlled combustion in an IC-engine with a fully variable valve train. SAE paper 2001-01-0251.
Li, S.C., Varatharajan, B.Williams, F.A., 2001. Chemistry of JP-10 ignition. Aiaa Journal **39**(12): 2351-2356.
Li, S.C.Williams, F.A., 1999. NOx formation in two-stage methane-air flames. Combustion and Flame **118**(3): 399-414.

Liang, L., Stevens, J.G., Farrell, J. T., 2008. A dynamic adaptive chemistry scheme for reactive flow computations. 32nd international symposium on combustion: In production progress.

Lindstedt, R.P., Meyer, M. P., 2003. A dimensionally reduced reaction mechanism for methanol oxidation. Proceedings of the Combustion Institute **29**: 1395-1402.

Lu, T.F., Ju, Y. G., Law, C. K., 2001. Complex CSP for chemistry reduction and analysis. Combustion and Flame **126**(1-2): 1445-1455.

Lu, T.F., Law, C. K., 2005. A directed relation graph method for mechanism reduction. Proceedings of the Combustion Institute **30**: 1333-1341.

Lu, T.F., Law, C.K., 2006a. Linear time reduction of large kinetic mechanisms with directed relation graph: n-Heptane and iso-octane. Combustion and Flame **144**(1-2): 24-36.

Lu, T.F., Law, C.K., 2006b. On the applicability of directed relation graphs to the reduction of reaction mechanisms. Combustion and Flame **146**(3): 472-483.

Lu, X.C., Chen, W.Huang, Z., 2005. A fundamental study on the control of the HCCI combustion and emissions by fuel design concept combined with controllable EGR. Part 2. Effect of operating conditions and EGR on HCCI combustion. Fuel **84**(9): 1084-1092.

Marchese, A.J., Dryer, F.L.Nayagam, V., 1999. Numerical modeling of isolated n-alkane droplet flames: Initial comparisons with ground and space-based microgravity experiments. Combustion and Flame **116**(3): 432-459.

Marriot, C.D., Reitz, R.D., 2001. Experimental Investigations of Direct Injection-Gasoline for Premixed Compression Ignited Combustion Phasing Control. SAE paper 2002-01-0418.

Mashayek, F., 1998. Direct numerical simulations of evaporating droplet dispersion in forced low Mach number turbulence. International Journal of Heat and Mass Transfer **41**(17): 2601-2617.

Mass, U., and Pope, S.B., 1992. Simplifying chemical kinetics: Intrinsic low dimensional manifold in composition space. Combustion and Flame **88**: 239-264.

Mehl, M., H. J. Curran, W. J. Pitz and C. K. Westbrook. 2009a. Chemical kinetic modeling of component mixtures relevant to gasoline. European Combustion Meeting, Vienna, Austria.

Mehl, M., W. J. Pitz, M. Sjöberg and J. E. Dec. 2009b. Detailed kinetic modeling of low-temperature heat release for PRF fuels in an HCCI engine. SAE Paper No. 2009-01-1806.

Mikolaitis, D.W., Segal, C.Chandy, A., 2003. Ignition delay for jet propellant 10/air and jet propellant 10/high-energy density fuel/air mixtures. Journal of Propulsion and Power **19**(4): 601-606.

Najt, P.M., Forster, D.E., 1983. Compression-Ignited Homogeneous Charge Combustion. SAE paper 830264.

Nakra, S., Green, R.J.Anderson, S.L., 2006. Thermal decomposition of JP-10 studied by micro-flowtube pyrolysis-mass spectrometry. Combustion and Flame **144**(4): 662-674.

Oevermann, M., Schmidt, H.Kerstein, A.R., 2008. Investigation of autoignition under thermal stratification using linear eddy modeling. Combustion and Flame **155**(3): 370-379.

Patterson, M.A., Kong, S.-C., Hampson. G. J. and Reitz, R. D., 1994. Modeling the effects of fuel injection characteristics on diesel engine soot and NOx emissions. Society of Automotive Engineers Technical Paper 940523.

Peters, N., 1988. Systematic reduction of flame kinetics - Principles and details. 11th International Colloquium on Dynamics of Explosions and Reactive Systems, Warsaw, Poland.

Petrova, M.V.Williams, F.A., 2006. A small detailed chemical-kinetic mechanism for hydrocarbon combustion. Combustion and Flame **144**(3): 526-544.

Petzold, L., Zhu, W. J., 1999. Model reduction for chemical kinetics: An optimization approach. Aiche Journal **45**(4): 869-886.

Pope, S.B., 1997. Computationally efficient implementation of combustion chemistry using in situ adaptive tabulation. Combustion Theory and Modelling **1**(1): 41-63.

Prasad, L.Skourikhine, A.N., 2005. Vectorized image segmentation via trixel agglomeration. Graph-Based Representations in Pattern Recognition, Proceedings **3434**: 12-22.

Prasad, L.Skourikhine, A.N., 2006. Vectorized image segmentation via trixel agglomeration. Pattern Recognition **39**(4): 501-514.

Rabitz, H., Kramer, M., Dacol, D., 1983. Sensitivity Analysis in Chemical Kinetics. Annual Review of Physical Chemistry **34**: 419-461.

Revel, J., Boettner, J.C., Cathonnet, M.Bachman, J.S., 1994. Derivation of a Global Chemical Kinetic Mechanism for Methane Ignition and Combustion. Journal De Chimie Physique Et De Physico-Chimie Biologique **91**(4): 365-382.

Reynolds, W.C., 1989. The potential and limitations of direct and large eddy simulation. Lecture notes in physics: 313.

Richter, H., Benish, T.G., Ayala, F.Howard, J.B., 2000. Kinetic modeling of the formation of polycyclic aromatic hydrocarbons. Abstracts of Papers of the American Chemical Society **219**: U679-U679.

Richter, H., Granata, S., Green, W. H., Howard, J. B., 2005. Detailed modeling of PAH and soot formation in a laminar premixed bezene/oxygen/argon low-pressure flame. Proceedings of the Combustion Institute **30**: 1397-1405.

Roesler, J.F., Yetter, R.A.Dryer, F.L., 1995. Kinetic Interactions of Co, Nox, and Hcl Emissions in Postcombustion Gases. Combustion and Flame **100**(3): 495-504.

Scheimer, G.W., Strauss, T. S. and Ritschder, U., 1995. Combustion in a swirl chamber diesel engine simulation by computational fluid dynamics. Society of Automotive Engineers Technical Paper 950280.

Schultz, M.Liberman, M., 1999. Topic Detection and Tracking using idf-Weighted Cosine Coefficient. Philadelphia, PA (United States), University of Pennsylvania

Schwer, D.A., Lu, P.S.Green, W.H., 2003. An adaptive chemistry approach to modeling complex kinetics in reacting flows. Combustion and Flame **133**(4): 451-465.

Sirignano, W.A., 1993. Fluid-Dynamics of Sprays - 1992 Freeman Scholar Lecture. Journal of Fluids Engineering-Transactions of the Asme **115**(3): 345-378.

Squires, K.D.Eaton, J.K., 1991. Measurements of Particle Dispersion Obtained from Direct Numerical Simulations of Isotropic Turbulence. Journal of Fluid Mechanics **226**: 1-35.

Tan, P.N., M. Steinbach, V. Kumar. 2005. Introduction to Data Mining, Addison-Wesley

Turanyi, T., 1990. Reduction of Large Reaction Mechanisms. New Journal of Chemistry **14**: 795-803.

Curriculum Vitae

Kaiyuan He

Chemical and Biochemical Engineering Department
98 Brett Road, Piscataway, NJ 08854
Rutgers, The State University of New Jersey
Email: heky@eden.rutgers.edu

Education

09/2006 – present	Ph.D candidate, Chemical and Biochemical Engineering Department, *Rutgers, The State University of New Jersey*
	Thesis Advisor: Dr. Ioannis (Yannis) P. Androulakis Dr. Marianthi G. Ierapetritou
	Thesis Topic: "*Development of Kinetic Model Reduction Framework and Its Application in Realistic Flow Calculation*"
09/2002 – 07/2006	BS in Biology and Biotechnology Department, *Tsinghua University*, Beijing, China
	Senior Design and Degree Thesis: "S*ynthesis Mechanism of Biodegradable Plastic Polyhydroxyalkanoate (PHA) in Microorganisms*"
	Research Advisor: Dr. George G. Chen

Journal Publications

1. **He K.**, Ierapetritou M.G., and Androulakis I.P., Kinetic Analysis of Complex Mechanisms Using Element Flux Analysis (Under review in *Computers & Chemical Engineering*)

2. **He K.**, Androulakis I.P., and Ierapetritou M.G., Numerical Investigation of Stratified HCCI Combustion with CFD and Detailed Chemical Kinetics Using On-the-fly Reduction (Under review in *Combustion Science and Technology*)

3. **He K.**, Androulakis I.P., and Ierapetritou M.G., A Multi-element Flux Analysis for the Incorporation of Detailed Kinetic Mechanisms in Reactive Simulations, *Energy & Fuels*, **24** (1): 309-317 (2010)

4. **He K.**, Ierapetritou M.G., and Androulakis I.P., Integration of On-the-fly Kinetic Reduction with Multidimensional CFD, *AIChE Journal*, in press, DOI: 10.1002/aic.12072 (2010)

5. **He K.**, Androulakis I.P., and Ierapetritou M.G., On-the-fly Reduction of Kinetic Mechanisms Using Element Flux Analysis, *Chemical Engineering Science*, **65** (3): 1173-1184 (2010)

6. **He K.**, Ierapetritou M.G., and Androulakis I.P., A Graph-based Approach for Developing Adaptive Representations of Complex Reaction Mechanisms, *Combustion and Flame,* **155** (4): 585-604 (2008)